Investigating the Role of the Perivascular Niche on Glioma Stem Cell Invasion in a Three-Dimensional Microfluidic Tumor Microenvironment Model

by

Emmanuella Akweley Adjei-Sowah

A Thesis Presented in Partial Fulfillment
of the Requirements for the Degree
Master of Science

Approved April 2020 by the
Graduate Supervisory Committee:

Mehdi Nikkhah, Chair
Christopher Plaisier
Shwetal Mehta

ARIZONA STATE UNIVERSITY

May 2020

ABSTRACT

Glioblastoma Multiforme (GBM) is a grade IV astrocytoma and the most aggressive form of cancer that begins within the brain. The two-year average survival rate of GBM in the United States of America is 25%, and it has a higher incidence in individuals within the ages of 45 - 60 years. GBM Tumor formation can either begin as normal brain cells or develop from an existing low-grade astrocytoma and are housed by the perivascular niche in the brain microenvironment. This niche allows for the persistence of a population of cells known as glioma stem cells (GSC) by supplying optimum growth conditions that build chemoresistance and cause recurrence of the tumor within two to five years of treatment. It has therefore become imperative to understand the role of the perivascular niche on GSCs through *in vitro* modelling in order to improve the efficiency of therapeutic treatment and increase the survival rate of patients with GBM.

In this study, a unique three dimensional (3D) microfluidic platform that permitted the study of intercellular interactions between three different cell types in the perivascular niche of the brain was developed and utilized for the first time. Specifically, human endothelial cells were embedded in a fibrin matrix and introduced into the vascular layer of the microfluidic platform. After spontaneous formation of a vascular layer, Normal Human Astrocytes and Patient derived GSC were embedded in a Matrigel® matrix and incorporated in the stroma and tumor regions of the microfluidic device respectively.

Using the established platform, migration, proliferation and stemness of GSCs studies were conducted. The findings obtained indicate that astrocytes in the perivascular niche significantly increase the migratory and proliferative properties of GSCs in the tumor microenvironment, consistent with previous in vivo findings.

The novel GBM tumor microenvironment developed herein, could be utilized for further in-depth cellular and molecular level studies to dissect the influence of individual factors within the tumor niche on GSCs biology, and could serve as a model for developing targeted therapies.

DEDICATION

I dedicate my work to my twin brother, Emmanuel Oko Sowah Adjei, and my best friend and confidante, Daniel Brenya Adjei.

ACKNOWLEDGMENTS

My sincerest gratitude first goes to Dr. Mehdi Nikkhah for giving me the opportunity to study and build myself under his mentorship these past years. I am grateful for all the guidance and support he provided despite my lack of experience, and most especially, the patience and confidence he had for me towards this project.

I am also grateful to all members of the Nikkhah Lab, especially Jaime Veldhuizen for helping me with all my wafer developments and trainings, and Eric Barrientos for teaching me basic lab practices when I first joined the lab.

I am also very grateful to my committee members, Dr. Shwetal Mehta and Dr. Christopher Plaisier for all their guidance and support. Thank you for holding very long discussions with me to discuss my data and provide input on subsequent steps. Without your support **on** every step of the way, I would not have been able to successfully complete my thesis.

Special thanks to Farbod Amir Ghasemi, Dr. Jin Park and Alejandra Patino, for helping me and giving me valuable inputs these past years.

TABLE OF CONTENTS

CHAPTER Page

LIST OF TABLES

LIST OF FIGURES

LIST OF ABREVIATIONS

2D	Two dimensional
3D	Three dimensional
ABM	Astrocyte Basal Medium
BBB	Blood Brain Barrier
BMP	Bone Morphogenic Protein
BSA	Bovine Serum Albumin
CD	Cluster of Differentiation
CNS	Central Nervous System
DAPI	4’,6-diamidino-2-phenylindole
DI	De Ionized
DMEM	Dulbecco’s Modified Eagle’s Medium
DMSO	Dimethylsulfoxide
DPBS	Dulbecco’s Phosphate Buffered Saline
ECM	Extracellular matrix
EdU	5-ethynyl-2’-deoxyuridine
EGFR	anti-Epidermal Growth Factor Receptor
EGM-2	Endothelial Growth Medium
FBS	Fetal Bovine Serum
FGF	Fibroblast Growth Factor
FOV	Field of View
FU	Fibrinolytic Units
GA	Glutaraldehyde
GAM	Glioma Associated Macrophages
GBM	Glioblastoma Multiforme
GFAP	Glial Fibrillary Acidic Protein
GIC	Glioma Initiating Cells

GJC	Gap Junctional Communication
GSC	Glioma Stem Cell
hEGF /EGF	human Epidermal Growth Factor
HUVEC	Human Umbilical Vein Endothelial Cell
IF	Immunofluorescence
LM	Laminin
MMP	Matrix Metalloprotease
MTCS	Methyltriclorosilane
NHA	Normal Human Astrocytes
NSC	Neural Stem Cell
NSPC	Neural Stem Progenitor Cells
PDGF	Platelet Derived Growth Factor
PDL	Poly-D-Lysine
PDMS	Polydimethylsiloxane
PFA	Parafomaldehyde
RFP	Red Fluorescent Protein
RNA	Ribonucleic Acid
RPM	Rotations Per Minute
RT	Room Temperature
SHH	Sonic Hedgehog
TME	Tumor Micro Environment
TMZ	Temozolomide
UV	Ultraviolet
VEGF	Vascular Endothelial Growth Factor
WHO	World Health Organization

CHAPTER 1

INTRODUCTION AND BACKGROUND

1.1 GLIOBLASTOMA MULTIFORME

A glioma is a term that is generally used to classify primary tumors depending on their supposed cell of origin or cause. These gliomas account for about 80% of malignant primary brain tumors and are therefore the most occurring tumors of the Central Nervous System (CNS) (Omuro & DeAngelis). Typical examples of gliomas include oligodendrogliomas, ependymomas, and astrocytic tumors. The most malignant of all these various types of tumors is glioblastoma multiforme (GBM), which is a type of primary astrocytoma (Taylor, Brzozowski, & Skelding). Patients who are diagnosed with GBM generally have a 25% survival time of 12 months, and 5% average survival time of five years.

In 2016, the American Brain Tumor Association predicted about 24,790 new cases of glioblastoma annually, with a higher incidence in men and in age ranges 45-65 years. Although the causes of glioblastoma remain unknown, it was proven that they can be caused by genetically inherited syndromes like Neurofibromatosis, Li-Frameni and Von Hippel-Lindau which only affect 5% of the total patient population. According to the World Health Organization (WHO), GBM has been classified as a Grade IV tumor, meaning that it is the most aggressive, invasive and malignant type of tumor. These characteristics contribute to its high resistance to conventional therapies, and consequently its low survival rate (Bahadur, Sahu, Baghel, & Saha)

Over the years, treatment options for GBM have continued to increase, however, not much progress has been seen. This is because, GBM is a very heterogenic tumor with neoangiogenic and intratumoral hallmarks (Shergalis, Bankhead, Luesakul, Muangsin, & Neamati). The Neoangiogenic hallmark allows the creation of new blood vessels for the tumors that enhances their growth and malignancy. These new blood vessels are rather leaky, and therefore permit further progression of the cancer (Hanif, Muzaffar, Perveen, Malhi, & Simjee Sh) Despite this heterogeneity, conventional therapies for GBM have focused on general eradication of the tumors by administering drugs like temozolomide and curcumin. For instance, in a study by Bahadur *et al*,

the combined effects of temozolomide and other drugs were studied, in an attempt to reduce the side effects of TMZ, while altering the drug delivery manner. Although combined therapies of temozolomide and radiotherapy doubled the 2-year survival rate, long term exposure to temozolomide builds resistance against malignant tumors and therefore reduces the efficiency of these drugs, leading to tumor recurrence (Bahadur et al.). In another study by Branter *et al*, medium frequency alternating electric fields were administered to tumors in an attempt to disrupt actively dividing cancer cells (Branter *et al*.). However, this therapy has to be used in combination with other therapies since it does not eradicate the glioma stem cells (GSC) population which contribute to the recurrence of the tumor (Taylor et al.).

Although these approaches have produced results, the survival rate for GBM still remains very low mainly due to interpatient heterogeneity (Shergalis et al.). In fact, GBM has been classified into four main subtypes including; classical, mesenchymal, proneural and neural types (Omuro & DeAngelis). The classical GBM phenotype is characterized by chromosome 10 deletions, chromosome 7 amplifications, EGFR mutations, EGFR amplifications, and Ink4a/ARF locus deletion (Phillips et al.). Alternatively, the mesenchymal phenotype is characterized by a high occurrence of genes involved in the tumor necrosis factor pathways and other genes like CHI3L1 and MET which are types of proto-oncogenes responsible for cell growth and survival (Phillips et al.). Furthermore, the proneural GBM subclass is characterized by mutations in genes like Tumor Protein 53 (TP53), a tumor suppressor gene responsible for cell division regulation and the isocitrate dehydrogenase 1 (IDH1) gene. Lastly, the neural subclass is characterized by the expression of neuronal makers like Nestin and beta-III Tubulin (Henrik Heiland et al.).

These subclasses shed more light on the different classes of GBM, and a deeper understanding of them can advise about targeted therapy treatment options (Baxter et al.). For instance, in a study by Hata *et al*, the contributory effects of bevacizumab and temozolomide in IDH-wild type glioblastoma was investigated (Okada et al.). BEV was used as a first line treatment in these patients, and it was found to prolong patient survival when used in combination with TMZ. In another study by Gravina *et al*, the small molecule Ephrin Receptor Inhibitor, GLPG1790 was administered to tumors to reduce the self-renewal capabilities of these cells (Gravina et al.).

Although this treatment was effective in reducing the tumor size in U251MG and U87MG subcutaneous xenograft models, it was found that GLPG1790 was not as effective as conventional combinatorial therapies. Hence, further research regarding the dosage and cytotoxicity is required (Henrik Heiland et al.).

Altogether, a major underlying factor of the setbacks observed in GBM prognosis can be evidently attributed to the presence of a glioma stem cell (GSC) population in the primary tumors (Wolf et al.). These GSCs are characteristic of the initiation, progression and recurrence of the tumors and are therefore responsible for the low survival rate of GBM (Hanif et al.). Therefore, therapies which aim at eradicating these GSC populations can produce good results.

1.2 GLIOMA STEM CELLS AND THE TUMOR MICROENVIRONMENT

Glioma stem cells (GSCs) are a small population of slowly-dividing, therapy resistant malignant cells found within the primary tumor. They are responsible for the initiation of GBM, the progression and maintenance of the tumor, as well and the recurrence of the tumor (Abou-Antoun, Hale, Lathia, & Dombrowski). They also have the ability to self-renew, proliferate for an unspecified period of time and to differentiate into any cell type of the same lineage, similar to neural stem cells (NSC). In this regard, they express various NSC markers like Nestin, SOX2 and CD133, while also maintaining the neoplastic clone characteristic (Ahmed, Auffinger, & Lesniak). Due to these characteristics, as well as their high chemotherapy and radio-resistance, they are believed to be the driving force behind GBM relapses. Although the true origin of these GSCs remain a mystery, scientists believe that they could originate from the proliferation of neural stem cells, dedifferentiation of neural cells or the transformation of undifferentiated precursor cells (Friedmann-Morvinski & Verma). The first population of Neural Stem Progenitor Cells (NSPCs) were first isolated by Uchida's group using the CD133 cell surface (Uchida et al.). Following that, multiple studies have proven the existence of GSC in the tumor mass. Additionally, a number of pathways have been associated with the presence of glioma stem cells including, but not limited to the Notch Signaling pathway, Sonic hedgehog and Wnt signaling pathway.

Normally, the notch signaling pathway is responsible for determining cell fate, proliferation and migration, as well as regulation of neural cell differentiation and cellular (Bazzoni and

Bentivegna). GSCs express high amounts of Notch signaling pathway activators like Fatty acid-binding protein 7 (FABP&) and Inhibitor of Differentiation 4 (IDF4) and consequently promote GBM invasion and growth. Also, Notch signaling has been proven to maintain stemness of GSCs as well as involvement in determination of glial cell fate (Sato et al.).

The Sonic Hedgehog signaling pathway is primarily responsible for neural progenitor regulation and organogenesis in embryonic development (Clement, Sanchez, de Tribolet, Radovanovic, & Ruiz i Altaba). GSCs have been shown to activate the SHH pathway which leads to a chain reaction involving the expression of Nanog (Abou-Antoun et al.), the loss of p53, downregulation of GL1 activity (Ma et al.) and ultimately, the maintenance of stemness (Zbinden et al.).

The Wnt pathway is responsible for the self-renewal and differentiation of NSCs as well as the differentiation of the interior and posterior structure of the Central Nervous System (CNS). A disturbance in the Wnt pathway activity leads to stemness programming and maintenance of GSCs through genetic and epigenetic mechanisms (Su et al.). Specifically, the upregulation of the zinc finger protein transcription factor, PLAGL2, leads to the upregulation of other Wnt components like Wnt6 and the activation of the canonical Wnt pathway, which ultimately results in an enhanced conducive microenvironment for the maintenance of GSCs (Su et al.).

Based on the activities of these pathways alone, developing therapies to disrupt their mechanism of action can be beneficial in eliminating GSCs (Ahmed et al.). For instance, by targeting the SHH pathway, we can improve chemotherapy efficacy because the SHH causes the downregulation of BMP, which leads to enhanced GSC proliferation. Hence, by inhibiting the SHH pathway, we can eliminate the contributory chemo resistant property of SHH pathway (Sharifzad et al.). Also, by targeting the Wnt axis at the tumor level, we can disrupt the canonical pathway responsible for providing a conducive environment for the GSCs, and thereby reduce the survival of the GSCs to the barest minimum (Zuccarini et al.)

However, besides the genetic mechanisms underlying GSC activity, epigenetic heterogeneity also plays a very significant and complex role in GSC survival. Other than causing mutations in histone modifications, epigenetic mechanisms lead to hypermethylation and

hypomethylation of tumor suppressor genes and oncogenes respectively (Tessarz & Kouzarides). These activities contribute to GBM development by promoting tumor growth and formation, and therefore, only by effectively targeting these mechanisms, can treatments become effective.

For example, in a recent study, Ulasov *et al* investigated the response of GSCs to TMZ after inhibition of SHH and Notch pathways in $CD133^+$ cells (Ulasov, Nandi, Dey, Sonabend, & Lesniak). Specifically, $CD133^+$ Notch and SHH cells were enriched for through transcriptional analysis. Notch and SHH pathways were inhibited through exposure to GSI-1 and cyclopamine respectively, after which the cells were treated with TMZ (Ulasov et al.). While the inhibition of the two pathways led to the enhanced therapeutic effects of TMZ, it also led to a significant upregulation of $CD133^+$ glioma cytotoxicity which further proved the contributory chemo resistant activities of these pathways (Ulasov et al.).

Furthermore, Matsuda's team investigated the inhibition of the JNK pathway in patient derived TGS01 cells and showed that the depletion of stem-like glioma cells was linked to the inhibition of this pathway. It was proven that the JNK pathway was also responsible for the self-renewal, tumor initiation property and maintenance of stemness in GSCs (Matsuda et al.). In another study by Sato *et al*, metformin, which is an antidiabetic agent was used to activate FOXO3. Activation of FOXO3 allowed for cell differentiation through the AMP-activated protein kinase (AMPK) activation pathway, which consequently led to the depletion of GSC-like cells in the tumor by eliminating the self-renewing, proliferative population in the xenograft model (Sato et al.). Ultimately, it is evident that GSCs play a very crucial role in GBM progression and development. Although the genetic and epigenetic activities are the underlying mechanisms behind GSC survival, they are still complementary to the tumor microenvironment, which also plays a very significant role in GBM progression (Polyak & Hahn).

In a general sense, the tumor microenvironment (TME) refers to the immediate surrounding environment of a tumor, which is primarily made up of the Extra Cellular Matrix (ECM), immune cells, signaling molecules, fibroblasts and blood vessels (Polyak & Hahn) (**Figure 1.1).** The tumor and its microenvironment interact very closely and influence each other by transmitting extracellular signals which enhance tumor growth and metastasis, while influencing the evolution of the

cancerous cells (Silver & Lathia).

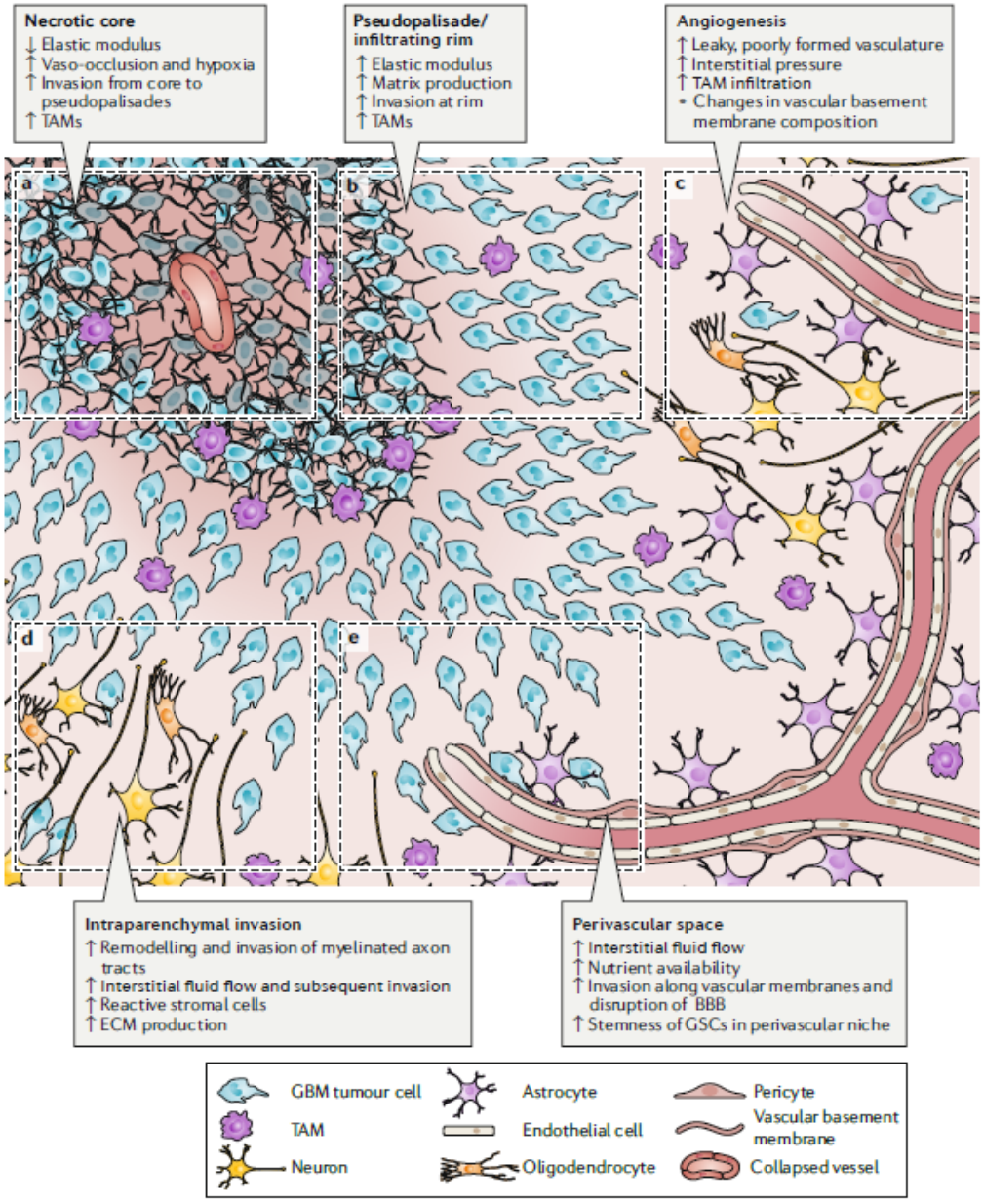

Figure 1.1: Glioblastoma tumor microenvironment (TME). **(a)** Schematic showing necrotic core **(b)** Pseudopalisade/infiltrating rim of GBM TME **(c)** Angiogenesis in perivascular niche **(d)** Intraparenchymal invasion area of GBM **(e)** Perivascular niche characterized by vasculogenesis and stroma cells. Adapted from Wolf et al. with permission from Nature Reviews Materials, copyright (2019) (Wolf et al. 2019)

1.2.1 VARIOUS NICHES IN THE TUMOR MICROENVIRONMENT (TME)

The GBM tumor microenvironment is no exception and has been characterized into specific niches including the perivascular niche, the hypoxic niche, and the invasive niche **(Figure 1.1)**.

The hypoxic/perinecrotic niche is characterized by insufficient blood supply which leads to hypoxia and causes high permeability and the absence of smooth muscles. This causes pseudo- palisading necrosis and ultimately leads to enhanced tumor growth and glioma stem cell maintenance (Mathiisen, Lehre, Danbolt, & Ottersen). Furthermore, in the absence of adequate amounts of oxygen, Hypoxia-inducible factors (HIF1 and HIF2) proteins are upregulated, and subsequently cause the upregulation of IL-8 and VEGF, which further cause angiogenesis. These proteins also cause the activation of specific genes responsible for dedifferentiation and GSC maintenance, and hence the GSCs are able to self-renew and cause tumor recurrence even after chemotherapy (Silver & Lathia).

While the hypoxic niche allows for GSC maintenance and self-renewal, the invasive niche permits the GSCs to migrate and proliferate, thereby promoting tumor growth and invasiveness (Mathiisen et al.) **(Figure 1.1).** The invasive niche is characterized by a high population of astrocytes, pericytes and other microglial cells that cover more that 99% of the cerebrovascular surface (Hambardzumyan & Bergers), an important process which ensures the transfer of molecules and ions across the blood brain barrier (BBB). In the invasive niche, the blood vessels are almost completely surrounded by the GSCs, and they are more functional, as compared to the perivascular niche where they are mostly surrounded by stromal cells **(Figure 1.1)**. It is therefore evident that although the three main GBM niches may comprise of the same components, they all contribute to tumor progression in different manners (Hambardzumyan & Bergers). The perivascular niche consists of various cells and growth factors which lead to angiogenesis and increase tumor invasion (Calabrese et al.). It is further discussed in detail below.

1.3 THE PERIVASCULAR NICHE

The perivascular niche is characterized by a variety of cells including non-malignant cells like astrocytes and fibroblasts, immune cells, GSCs, and most importantly, blood vessels. Due to the abundance of a cocktail of growth factors like Vascular Endothelial Growth Factor (VEGF), Fibroblast Growth Factor (FGF) and Platelet Derived Growth Factor (PDGF), the perivascular niche is a very important element in GBM survival and progression (Hambardzumyan & Bergers). These growth factors affect the supply of oxygen to the tumor, result in hypoxia, and lead to the

formation of new blood vessels, a concept known as angiogenesis (Calabrese et al.). Most importantly, the perivascular niche is characterized by the formation of leaky blood vessels which result from the upregulation of VEGF. The leaky blood vessels in turn result in tumor progression by attracting immunomodulatory cells which suppress immune function (Plaks, Kong, & Werb). Tumor Associated Macrophages also serve a very important role in the perivascular niche. They are responsible for promoting GSC proliferation by inducing matrix metalloproteinase 9 (MMP9) and the simultaneous release of transforming growth factor -beta (TGF-β) (Hambardzumyan & Bergers).

All in all, the tumor microenvironment plays a critical role in tumor progression, and hence the disruption of this environment can lead to better treatment options for patients. For instance, a study by Truong *et al.* investigated the stemness and migratory abilities of the GB3 patient derived cell line in the presence of vasculature. Through his study, he confirmed the role of CXCL12 signaling pathway in GSC invasion by counteracting with AMD3100 (D. Truong et al.).

In another study by Infanger *et al*, the role of the vascular layer in the perivascular niche was further confirmed by studying the influence of the paracrine interleukin (IL)-8 signaling on cancer stem cells (CSCs) embedded in a scaffold-based culture system (Infanger et al.). Although these studies have proven that the perivascular niche is a very important tool in GBM tumor progression, there still remains unanswered questions due to a lack of a physiologically relevant platform that can adequately mimic the perivascular niche, and therein lies the relevance of this study.

1.4 MODELS FOR STUDYING GBM TUMOR PROGRESSION AND INVASION

To properly study GBM tumor progression, many scientists have engineered several platforms depending on the aim of the research and availability of resources. These platforms include Patient Derived Xenograft (PDX) models and *in vitro* methods.

1.4.1 In vivo models:

In vivo models have been instrumental for studying disease progression and drug studies. They present the advantage of closely mimicking the human and therefore produce physiologically relevant data. For example, in a study by Joo *et al*, glioblastoma xenograft models were used to

model the progression of glioblastoma in situ (Joo et al.). However, they pose huge ethical concerns in research, lack the normal human immune response, and are also very expensive, hence, only limited research can be conducted.

1.4.2 2D In vitro models:

In an attempt to address the concerns posed by the *in vivo* models, 2D *in vitro* models were used. Although these models are comparatively less expensive, they lack the physiologically relevant advantage presented by *in vivo* platforms. Due to this, most research performed on 2D platforms are not translative and still require further PDX experimental models. Some of these platforms include the transwell systems and micropatterning **(Figure 1.2 a-c)**. For example, Calabrese's group conducted a study to investigate the intercellular interactions between endothelial cells and glioma cells. By using a transwell assay system, the migration of glioma cells was studied. However, the morphology of the glioma cells in the 2D transwell platform varied from that in the 3D platform, indicating that the 2D platform lacked the necessary mechanical cues present in the 3D TME (Calabrese et al.).

Although these platforms are beneficial to some extent, they still present many disadvantages. They are end-point assays, and therefore do not allow for the real time visualizations of cellular interactions during the course of the experiments. Most importantly, they do not properly recapitulate the TME because they are two-dimensional (2D) assays, whereas the brain microenvironment is a three-dimensional (3D) environment with various cues. Due to this, they lack physiological relevance because the cells behave differently in a 2D environment as compared to a 3D environment, hence, results obtained from performing these assays are not translative to results obtained from *in vivo* studies. Furthermore, they consume a lot of resources like cells, cell culture media, etc. because of the sizes of experiments which makes them expensive to use.

1.4.3 Microfluidic and hydrogel-based 3D model for tumor microenvironment glioblastoma invasion studies:

Despite significant advances made in developing appropriate platforms for GBM studies, there is still a lack of a physiologically relevant model to recapitulate the TME. To date, numerous

efforts have utilized 3D micro engineered surface topographies, 3D hydrogel-based biomaterials, 3D bioprinting models, as well as 3D microfluidics platforms for specific applications in regenerative medicine, vascularization, tissue engineering, disease modeling and cancer cell behavior studies. (Saini, Navaei, Van Putten, & Nikkhah) (Peela et al.) (Peela, Truong, et al.; Strobl, Nikkhah, & Agah) (Memic et al.) (Truong et al.) (Nikkhah, Strobl, Peddi, & Agah) (A. Navaei et al.) (Pal, Vernon, & Nikkhah) (Nikkhah, Strobl, De Vita, & Agah) (Pal et al.) These models have also provided unprecedent ability to mimic the complexities of the native tissue microenvironment in healthy and diseased states (Nikkhah et al.) (Ali Navaei et al.) (Pedde et al.) (Kharaziha et al.; Nagaraju, Truong, Mouneimne, & Nikkhah) (A. Navaei, Truong, et al.; Saini et al.) (Cha et al.) (Kharaziha et al.) (Saini et al.). Some specific applications for GBM TME modeling and inculcation of mechanical and biochemical cues observed in the brain have been demonstrated in **Figure 1.2 f-h.**

A study by Wang's team showed the interdependence of patient derived glioma cells on endothelial cells by creating a tumor-endothelial microenvironment and investigating the proliferative and morphological properties of the cancer cells. After embedding endothelial cells into 3D vessel-like hydrogel structures, they were cocultured with patient derived GBM cells. They observed no significant differences in proliferation across their experimental conditions, and this observation was attributed to a lack of additional cues or stimulus that are normally present in the tumor microenvironment (C. Wang et al.).

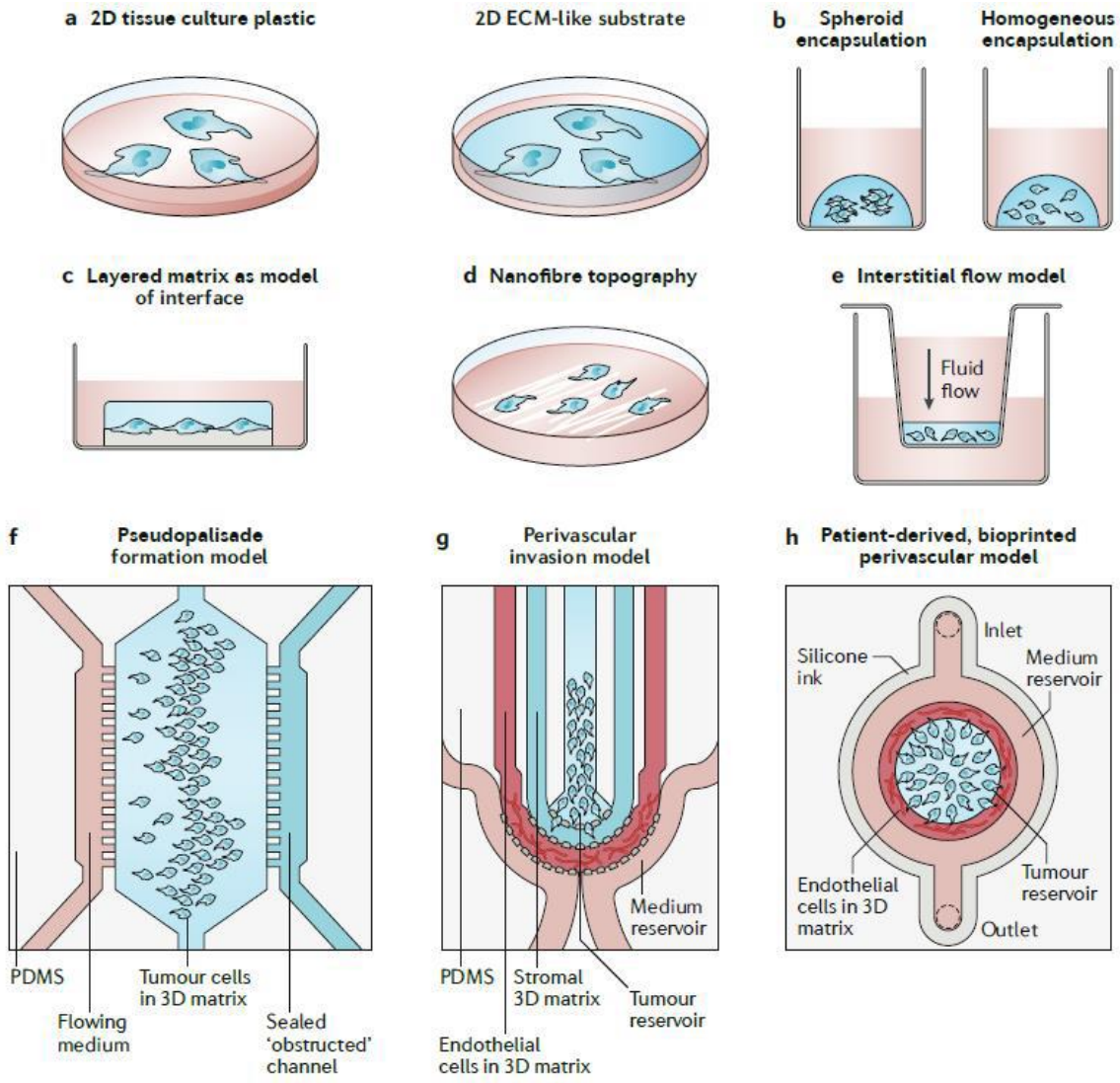

Figure 1.2: Examples of two-dimensional and three-dimensional models for GBM tumor progression studies. **(a)** Schematic showing 2D culture of cells in tissue culture plastic and on an ECM substrate **(b)** Schematic showing gel encapsulation of cells in a tissue culture flask **(c)** Schematic showing a layered matrix model of cells in a tissue culture plastic **(d)** Schematic showing nanofiber topography model **(e)** Schematic showing interstitial flow model for GBM invasion studies **(f)** Schematic showing microfluidic model for studying pseudo palisade formation **(g)** Schematic showing microfluidic model for studying glioma stem cell invasion in the perivascular niche **(h)** Schematic showing 3D bioprinted model for studying glioma stem cell invasion in the perivascular niche. Adapted from Wolf et al. with permission from Nature Review Materials (2019) (Wolf et al. 2019).

In another study, Heinrich *et al* developed a 3D platform to study the crosstalk between glioblastoma and glioma associated macrophages. In this study, a 3D-bioprinted tumor model was engineered by first printing and encapsulating mouse macrophage cells in a large brain model, and

then filling the empty cavity in the large brain model with mouse glioblastoma cells embedded in bioink. The 3D printed tumor model enabled the study of interactions between GAMs and Glioma cells through expressions of specific markers like Mrc1 and GFAP (Heinrich et al.).

In a more recent study, Yi's group investigated the response of glioma cells to chemotherapy on a 3D bioprinted chip model. Specifically, a brain derived ECM solution was developed and used to print the GBM-on-a-chip model. By establishing an oxygen gradient, Yi's group was able to establish the core, intermediate and peripheral regions in the hypoxic niche, similar to the *in vivo* environment **(Figure 1.3 a)** (Yi et al.)**.** Although this model was effective in mimicking the hypoxia niche of the GBM TME, it did very little to mimic the perivascular niche due to the lack of a well-formed vascular layer and the absence of stromal cells which form a very important part of the GBM TME **(Figure 1.3 b).** To address these concerns, complex models which allow for biochemical, biophysical and mechanical cues similar to the GBM TME need to be established.

Various 3D models have been used to study disease progression and various contributory factors of the *in vivo microenvironment.* (Nikkhah, Strobl, Schmelz, & Agah) (A. Navaei, Saini, et al.) (Fidoamore et al.) (Bertassoni et al.) (Nikkhah, Strobl, Schmelz, Roberts, et al.) (Dolatshahi-Pirouz, Nikkhah, Kolind, Dokmeci, & Khademhosseini) (Zorlutuna et al.) (Nikkhah, Strobl, & Agah). Specifically, microfluidics models have been proven as powerful technologies and have been used in various disease modeling studies. However, only recently have a few studies started to focus around GBM and the TME. As such, there still exists numerous unanswered questions about GSCs behavior in the TME. By using microfluids, the GBM TME can be properly recapitulated. Furthermore, real time imaging of cellular interactions can be observed due to the transparent nature of the materials used to make the microfluidic devices. Also, these microfluidic devices are very easy and low cost to make, hence resources can be saved and used efficiently. Furthermore, since these platforms are engineered at the micro-level, they require lesser number of cells and cell culture materials as compared to the 2D *in vitro* models (Truong et al.) (D. D. Truong et al.).

In a study by Ayuso *et al*, a newly developed microfluidic model was used to study GBM aggressiveness after altering the tumor microenvironment. In brief, microfluidic devices were

developed through SU-8 photolithography. The device composed of two channels, namely the thrombotic and perfused channel, and a microchamber for the culture of cells (Ayuso et al.). U-251-Mg cells were embedded in freshly prepared collagen matrix and injected into microfluidic devices. To mimic the pseudopalisade concept, the microfluidic devices were placed in an already prepared packaging tool after 24 hours, and all but one pair of device inlets were sealed **(Figure 1.2 f 1.3 c).**

During a 9-day experimental period, the migratory tendencies of the U-251-Mg cells were monitored. Ayuso's team observed increased migration in conditions with obstructed medium flow, while conditions with unrestricted medium flow were seen to have a uniform distribution of cells in the devices. Furthermore, it was observed that, under obstructed conditions, a larger population of the cells were positive for ki-67, as against unrestricted conditions **(Figure 1.3 d).** These results indicate the relevance of blood vessels in the brain microenvironment by modelling blood flow, and further prove the contribution of the perivascular niche to tumor progression (Ayuso et al.).

In another study by Ma *et al*, a detachable microfluidic device was used to investigate the invasive properties of glioma cells, as well as their response to therapeutic drugs including temozolomide and resveratrol. In brief, the microfluidic devices were fabricated by soft lithography **(Figure 1.3 e).** The chip composed of a lower layer made of a concentration gradient generator in the form of a 4X4 matrix that allowed for effective drug studies. It also consisted of an upper glass cover layer which was coated with PDMS and served as the cell culture region of the device. For experimental purposes, U87 cells were cultured via hanging drop technology onto the cell culture region of the microfluidic device. After three days, the U87 spheroids were retracted and embedded in collagen for culture in the 4X4 array. To conduct drug studies, the inlets of the device were filled with each type of drug respectively. This platform allowed for the investigation of invasion, viability, proliferation and drug treatment of GBM cells **(Figure 1.3 f)** (Ma et al.) (Whiteside). However, the major setback was the fact that invasion, proliferation and drug treatment analysis could only be performed at the end of the experimental assay, and hence did not permit for real time monitoring of intercellular interactions. Also, the device permitted the culture of only one cell type, contrary to the TME which is made up of different cell times and biochemical cues (Hambardzumyan & Bergers).

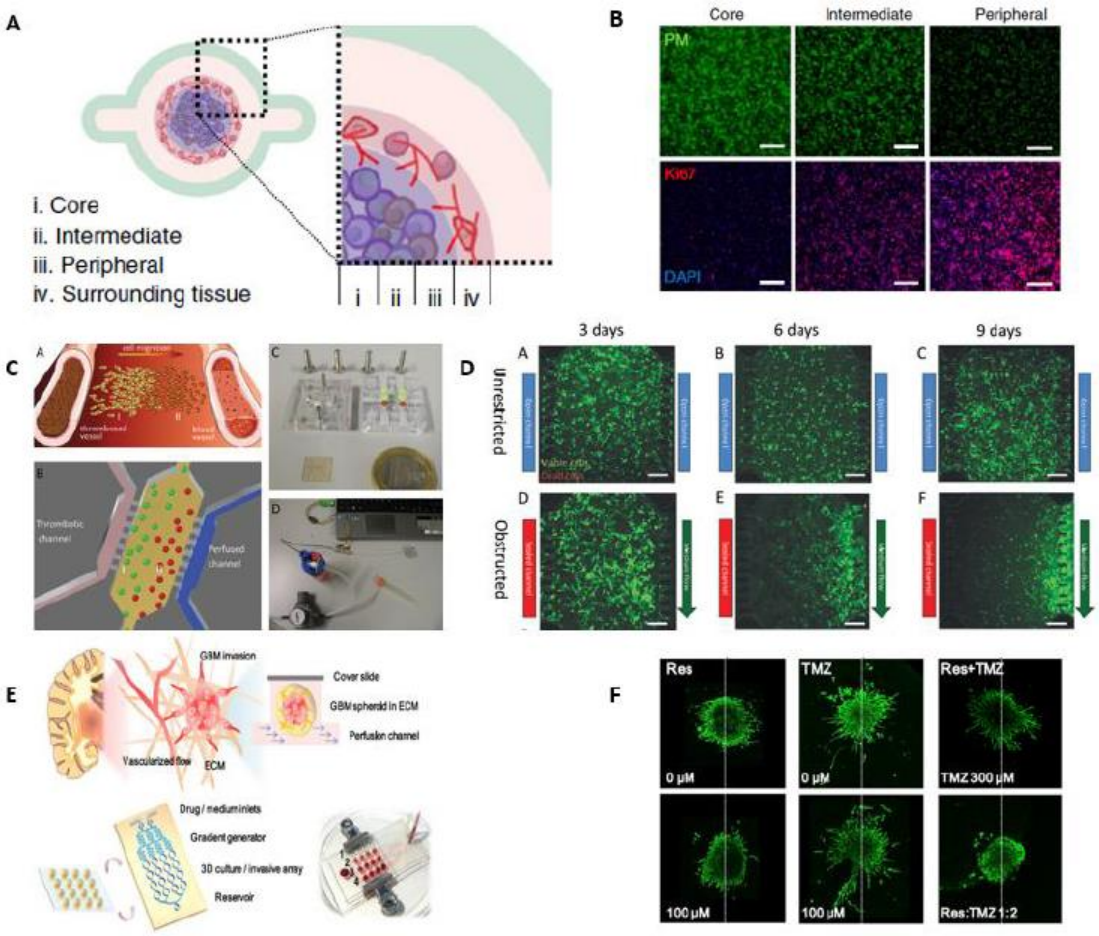

Figure 1.3: Examples of 3D microfluidic models to study glioblastoma invasion **(a)** Schematic showing bioprinted glioma-on-a-chip model **(b)** Immunofluorescence imaging of Ki-67 proliferative marker of glioma cells in the chip. Adapted from Yi et al with permission from Nature Biomedical Engineering, copyright (2019) (Yi et al. 2019) **(c)** Schematic showing microfluidic device for GBM pseudo palisade studies. **(d)** Fluorescent image showing distribution of glioma cells in microfluidic device Adapted from Ayuso et al with permission from Neuro oncology, copyright (2017) (Ayuso et al. 2017)). **(e)** Schematic showing glioblastoma tumor microenvironment and GBM TME model **(f)** Fluorescent images showing response of glioma cells to various drug concentrations. Adapted from Ma et al. with permission from Biomedical Microdevices copyright (2018) (Ma et al. 2018)

In a recent study by Chonan's group, a microfluidic device was developed to study GSC invasion in the presence of a formed blood vessel (Chonan, Taki, Sampetrean, Saya, & Sudo) **(Figure 1.4 a).** The microfluidic devices were fabricated using soft lithography techniques and were surface treated to promote attachment and polymerization of 3D hydrogels. They consisted of two

parallel channels separated by a type 1 collagen gel scaffold for cancer cell culture. After fabrication of microfluidic devices, an endothelial cell suspension was injected into one of the channels and cultured for three days to form a monolayer of cells. Following this, Glioma Initiating Cells (GIC) were embedded onto the collagen scaffold and allowed to grow for three days and invasive and proliferative properties of the GICs were studied **(Figure 1.4 b)** (Chonan et al.). Although this study allowed for the coculture of two cell types, it still lacked major biochemical and mechanical cues that are present in the TME, in that, endothelial cells used in this platform were made to form a 2D monolayer, contrary to the 3D blood vessel TME.

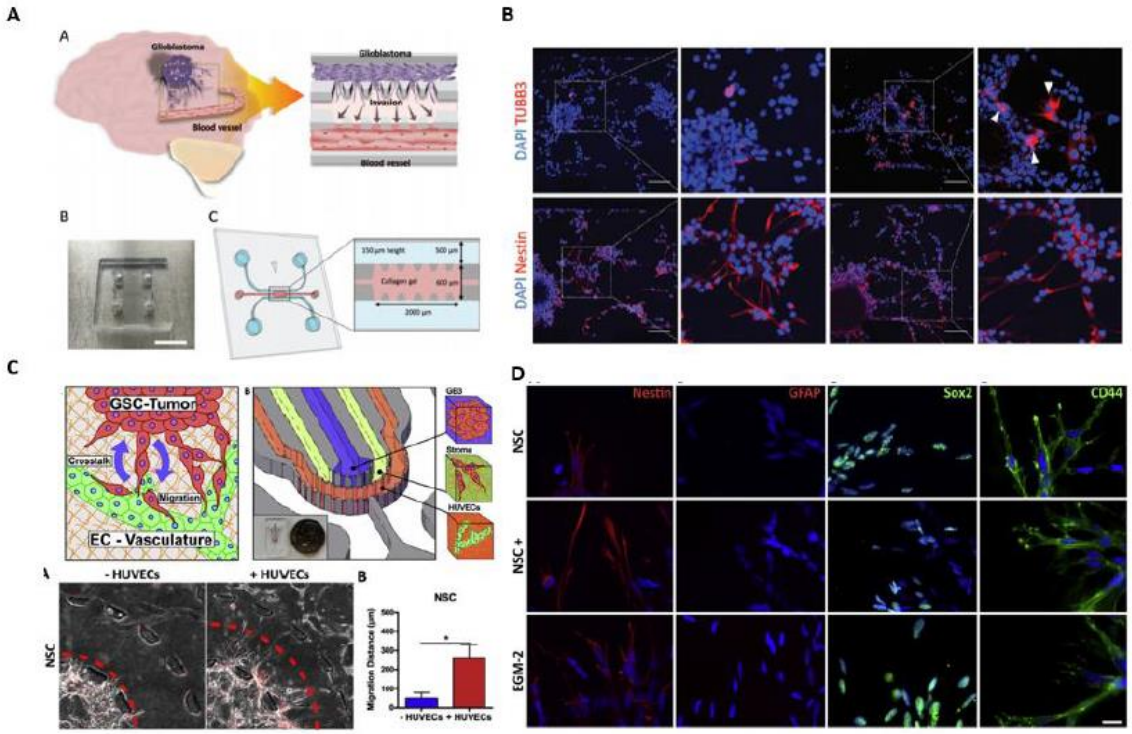

Figure 1.4: Examples of 3D microfluidic models to study glioblastoma invasion **(a)** Schematic showing tumor microenvironment and invasion of tumor to surrounding blood vessels **(b)** Fluorescent images showing expression Nestin of glioma cells in device. Adapted from Chonan et al with permission from Integrative biology, copyright (2017) (Chonan et al.) **(c)** Schematic showing microfluidic device with different layers for studying GBM tumor progression **(d)** Fluorescent images showing stemness of glioma cells in microfluidic device. Adapted with permission from Truong et al with permission from Biomaterials, copyright (2018) (D. Truong et al.).

To address these challenges, a 3D organotypic microfluidic device was engineered by

Truong's group (D. Truong et al.). In this study, a microfluidic device was fabricated using soft lithography techniques. Briefly, devices consisted of two media channels surrounding three cell culture channels namely tumor layer, stroma layer and vascular layer **(Figure 1.4 c)**. All channels were separated by evenly spaced trapezoidal microposts which permitted diffusion of nutrients and biochemical cues while allowing for a separated but interconnected platform. Following device fabrication, endothelial cells embedded in a fibrin matrix were injected into the vascular layer of the devices and allowed to spontaneously form blood vessels over a period of 72 hours. After a well-formed vascular layer was established, patient derived glioma stem cells were embedded in Matrigel® and injected into the tumor region of the devices. Over a three-day time period, the migration and morphological properties of the GSCs were monitored **(Figure 1.4 c)** (D. Truong et al.). Since the microfluidic devices were fabricated using PDMS and glass slides which are transparent, they allowed for real time imaging of intercellular interactions. This platform served as a good representation of the perivascular niche as it encompassed various biochemical and mechanical cues presented in the GBM TME **(Figure 1.4 d)**.

However, to properly mimic the perivascular niche, there still remains the need for a more physiologically relevant platform that incorporates more cell types found in the GBM TME. Stromal cells have been shown to play very important roles in tumor progression and development, hence the need to study their roles to gain more insight about how to curb tumor recurrence in the perivascular niche.

1.5 INFLUENCE OF STROMAL CELLS ON GLIOMA STEM CELL INVASION

Whereas various studies have focused on creating a physiologically relevant model to study GBM tumor progression and invasion by mimicking the perivascular niche, very few have investigated the contribution of stroma cells. Stroma cells like astrocytes and microglia play a very important role in maintaining and remodeling the ECM. Furthermore, astrocytes are involved in controlling the brains response to various forms of injury by regulating electrical synapse transmission in the brain (Faria et al.) (Rath, Fair, Jamal, Camphausen, & Tofilon).

To test this hypothesis, various studies have conducted 2D assays to prove the

involvement of astrocytes in GBM tumor progression. For example, in a study by Rath *et al*, astrocytes were cocultured with GSCs in a 2D transwell invasion assay. It was realized that the invasion capacity of the GSCs were greatly enhanced by the astrocytes. Furthermore, a gene expression analysis showed a modification in GSC expression after exposure to astrocytes in the transwell invasion assay for 48 hours, while an immunoblot assay also showed increased levels of proteins associated with GSC invasion and migration (Rath et al.).

In another study by Lin *et al*, astrocytes were shown to increase chemoresistance of glioma cells by upregulating specific genes associated with tumor survival, including tyrosine-protein kinase and mitogen-activated protein kinase (Lin, Liu, Ling, & Xu). Briefly, glioma cells were cultured in the presence or absence of astrocytes in a 2D assay after which microarray analysis was used to examine the gene expression patterns of the glioma cells (Lin et al.).

Previous studies attributed the chemoresistance of glioma cells to the leaky blood brain barrier, however, after further studies, it was concluded that this was not the sole cause of chemoresistance (Lin et al.). A number of signaling pathways like SHH and Wnt have been proven to increase chemoresistance of GSCs by upregulating genes related to. Under normal conditions, astrocytes function as housekeeping cells to maintain homeostasis in the TME, however, when an injury occurs, they change their mechanism of action and proceed to control the brains response to these injuries by altering the ECM (Henrik Heiland et al.). By acting as a responsive mechanism, several genes including GFAP are upregulated, and the astrocytes create a functional gap junctional communication (GJC) between themselves and the injury (tumor), which consequently leads to increased chemoresistance (Faria et al.). Lin's group confirmed that astrocytes had the ability to protect glioma cells from chemotherapy through GJC using microarray analysis (Lin et al.).

Without a doubt, stromal cells like astrocytes and microglia have been shown to contribute to the heterogeneity of GBM tumors (Hambardzumyan & Bergers). Microglia possess an M1 pro-inflammatory/M2 anti-inflammatory phenotype, however, in the presence of a tumor, this M1 phenotype is suppressed, and instead, an M2 anti-inflammatory phenotype is activated, which ultimately leads to the release of several chemokines and growth factors which cause tumor growth

(Hambardzumyan, Gutmann, & Kettenmann). Although the mechanism of action of microglial in tumor growth has been somewhat understood, that of astrocytes still remain unclear. However, in a recent study, it was shown that the behavior of astrocytes can be manipulated by GSCs and made to express a variety of factors like IL-10 and interferon beta which can lead to tumor growth (Guan, Hasan, Maniar, Jia, & Sun).

Broadly speaking, several factors are associated with astrocyte-glioma interactions including cytoskeletal arrangements, ECM alterations, neurotrophic and morphogenic factors, as well as chemokines, cytokines and metabolic factors (Matias et al.). The influence of these factors secreted by microglia on GBM tumor progression have been broadly studied, however, the influence of these factors in relation to astrocytes still remain unexplored. In this regard, a 3D model to investigate the influence of astrocytes on GBM tumor invasion has been developed for detailed studies.

In summary, although constructive studies have been conducted to study the role of the TME on glioma cells in various 2D and 3D platforms, there are still unanswered questions, specifically about the contribution of stromal cells in the perivascular niche to tumor progression in a well-defined 3D model that properly mimics the components in the perivascular niche. Previous studies that investigated the role of stromal cells on glioma cells either did so in a 2D model which has very low significance, or in a 3D model with the absence of the vascular layer (Faria et al.). Other studies that investigated the role of the hypoxic niche did not adequately model the perivascular niche, a very important factor in tumor progression, hence these knowledge gaps need to be properly addressed in a well-developed 3D *in vitro* model.

1.6 OBJECTIVE OF THE THESIS

The objective of this thesis was to investigate the role and contribution of the various components in the perivascular niche to GBM tumor progression. Specifically, a microfluidic platform was engineered based on an old model designed by Truong *et al* (D. Truong et al.). Using this model, astrocytes were cultured in the presence of a spontaneously formed vascular layer and a tumor region. Stromal cells have been hypothesized to be the point of linkage between GSCs and blood vessels in the perivascular niche. Therefore, by developing a model that allows for the

triculture of these cells, we aimed to properly investigate how the stromal cells promote GBM invasion and increase tumorigenicity in the TME.

Firstly, we proceeded to form a vascular layer in the engineered microfluidic platform based on previous protocols (D. Truong et al.). This involved injecting a mixture of HUVECs, fibrinogen and thrombin into the microfluidic device and allowing it to polymerize. Vasculogenesis was monitored over the course of 72 hours, after which the morphology and maturity of the spontaneously formed vascular layer was confirmed by staining for CD-31 and Actin filaments.

Following the establishment of the vascular layer, patient derived GSCs, namely GB3 cells, were incorporated adjacent to the vascular layer. Normal Human Astrocytes were then injected into the tumor-vascular models, and then invasion of GB3 cells were monitored for another 72 hours. To properly understand the contribution of astrocytes to GBM invasion, we employed four different experimental conditions namely;

1. Monoculture
2. Coculture with astrocytes
3. Coculture with vasculature
4. Triculture

All experimental assays were done based on these conditions. We also investigated how astrocytes influenced the stemness of the GSCs by staining for specific markers, through which we found that the GSCs maintained their stemness and proliferative properties.

All in all, this thesis shed insight on the influence of astrocytes on GSC invasion and tumor progression. Future work involves analyzing the various genes affected by the presence of the astrocytes, as well as exposing the developed platform to radiation therapy for drug studies. The engineered platform holds promising prospects, as the level of complexity can be further increased to resemble TME even more, and ultimately efficiently advise on drug treatment options for patients.

CHAPTER 2

ENGINEERING A MICROFLUIDIC PLATFORM TO MIMIC THE GBM PERIVASCULAR NICHE

2.1 INTRODUCTION

The tumor microenvironment (TME) is made up of several factors including the necrotic/hypoxic niche, the invasion niche, the perivascular niche, chemokines and cytokines, as well as growth factors (Sharifzad et al.). These various factors contribute to tumor growth and development. They also cause tumor initiation, progression and recurrence by building the chemoresistance of the tumor (Shergalis et al.). Specifically, a small population of cells known as glioma stem cells (GSCs) have been shown as the main drivers of tumor invasions. These GSCs are shielded by the various factors aforementioned, and therefore reserve the ability to proliferate and cause tumor recurrence (Hambardzumyan & Bergers) (Hanif et al.).

To properly study the TME, various *in vivo* and *in vitro* models have been developed. Although the *in vivo* model is attractive because they closely mimic the human body, they are very expensive and also present ethical issues. Furthermore, previous studies have shown that these *in vivo* models are not particularly translative to the human body. Therefore, scientists have engineered various 2D and 3D platforms for further studies (Peela, Barrientos, Truong, Mouneimne, & Nikkhah) (Peela, Truong, et al.) . Although these 2D models are useful to some extent, they are unable to produce translative data because they are not physiologically relevant. Hence, to properly model the tumor microenvironment (Peela et al.), a 3D model with biophysical, biochemical and mechanical cues is required . In regard to this, various 3D models like bioprinting, hanging drop technology and microfluidics have been engineered (Logun, Zhao, Mao, & Karumbaiah).

Of these 3D platforms, microfluidic devices are the most attractive due to their ability to provide a desirable 3D platform for the culture of as many cell types as possible (D. D. Truong et al.) . Previous studies have investigated the role of endothelial cells on GSC invasion, however, apart from modelling the tumor vasculature, no studies have been conducted to model other factors present in the tumor microenvironment.

In the study developed here, we engineered a microfluidic device based on a previous model proposed by Truong et al., which allowed us to culture multiple cell types simultaneously. Using this device, we mimicked the tumor microenvironment and studied the role of the perivascular niche on migration, proliferation and stemness of the glioma stem cell population (Nagaraju et al.) **(Figure 2.1).**

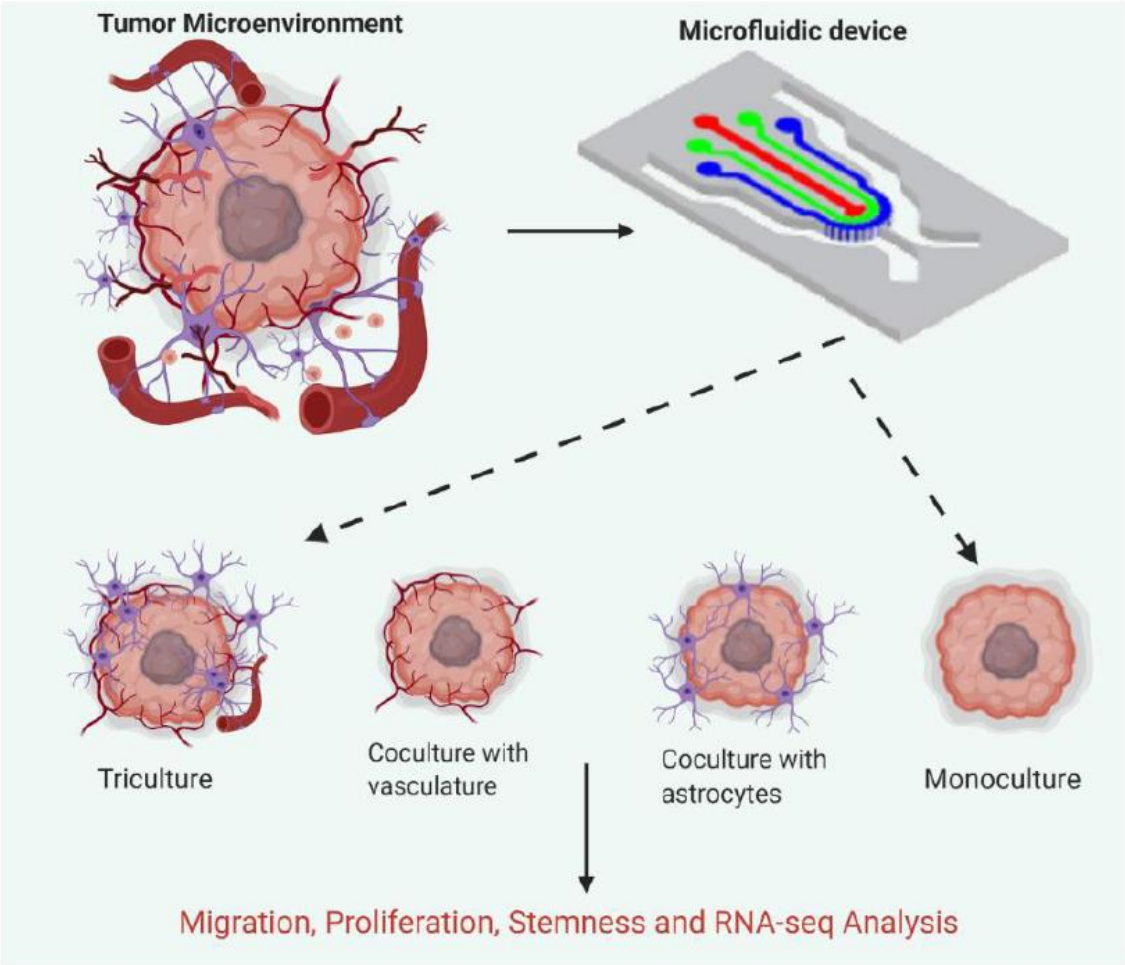

Figure 2.1: Timeline of experiment performed in engineered microfluidic platform. Schematic showing tumor microenvironment of glioma stem cells and schematic of microfluidic device. Tumor microenvironment is formed in the microfluidic devices under four conditions; monoculture, coculture with astrocytes, coculture with vasculature and triculture for a 6-day experimental period. After experimental period, Migration, proliferation, stemness and RNA-seq analysis is performed on all four conditions. *(*BioRender*)*

2.2 MATERIALS AND METHODS

2.2.1 Device design and fabrication:

a. Photolithography and Soft lithography for device fabrication

To make the microfluidic device, the desired pattern was created using CAD software and printed onto a transparent mask. Using SU8-2075 (Microchem) photolithography technology, a master mold was created by spinning to a height of 200µm onto the surface of a silicon wafer, after which the wafer with the underlying transparent mask was exposed to Ultraviolet (UV) to form a primary mold (insert Dans citation here). To make more devices, the surface of the silicon wafer was treated with Methyltrichlorosane (MTCS, Sigma-Aldrich) for some time. The purpose of this salinization treatment was to make the surface of the wafer hydrophobic to ensure easy retraction of the polydimethylsiloxane (PDMS, Slygard 184 Silicon Elastomer Kit, Dow Corning) after curing. A PDMS solution, mixed with curing agent in a 10:1 proportion was made and allowed to degas for 30 minutes, after which it was poured onto the salinized silicon wafer.

The wafer with the PDMS solution was then placed into an 80°C oven and allowed to cure for approximately 2 hours. Following this, the cured PDMS was retrieved from the wafer to make individual devices. The molds were then punched with 1mm and 2mm biopsy punches to create inlets and outlets. After this, the molds were cut out with a blade to separate individual molds.

To create channels, the PDMS molds were individually bonded to a 1mm thick glass slide. Briefly, the PDMS molds and glass slides were wiped with ethanol and pressurized nitrogen gas to rid of all particles and dirt. They were then arranged onto a petri dish and then treated with oxygen plasma (PDC-32G, Harrick Plasma) to ensure hydrophilicity. The devices were then bonded face down onto the glass slides and slightly pressed down to ensure attachment. Following this, the bonded devices were placed in an 80° C oven overnight to secure the bonds (Nagaraju et al.).

b. Sterilization

To ensure the devices were sterilized before use,, the devices were subsequently placed in a wet and dry autoclave, after which they were placed in an 80C oven and allowed to dry overnight.

c. Surface treatment

To restore hydrophobicity and ensure attachment of hydrogels to the channels, devices were treated with poly-d-lysine (1mg/ml) (PDL, Sigma-Aldrich) and Glutaraldehyde (1% (v/v)) (GA, Sigma-Aldrich). Specifically, PDL was injected into the cell culture channels and were kept at 37 C for 1 hour, after which the devices were washed once with DI water. GA was then introduced into the cell culture regions, incubated at room temperature for 1.5 - 2 hours, and then washed with DI water 3-5 times to ensure that there was no excess GA. Devices were then left in 80 C oven overnight to reintroduce hydrophobicity.

2.2.2 Cell culture:

Human Umbilical Vein Endothelial Cells (HUVEC, Lonza) were cultured in Endothelial Growth Medium (EGM-2, Lonza). Media was changed every other day, and cells were grown under standard conditions of 37 C, 5% CO2 and used at 70 - 80% confluency. HUVECs were only used between passages 3 – 7.

Patient samples were obtained as a gift from the Biobank Core Facility at St. Joseph's Hospital and Medical Center and Barrow Neurological Institute (BNI), Phoenix, Arizona (D. Truong et al.). Normal Human Astrocytes (NHA) cells were grown in Astrocyte Basal Medium (Glutamax, Fisher Science) supplemented with N2 (Fisher Science) and 10% Fetal Bovine Serum (FBS, Fisher Science). Media was changed every other day, and cells were only used between passages 4 - 10. NHA cells were used for 3D cultures at 70 - 80% confluency.

GB3 cells were obtained from resected primary GBM tumor tissue at BNI following previous protocols. GB3 cells were grown as spheroids in Neural Stem Cell (NSC) medium consisting of DMEM and F12-Glutamax supplemented with N2, B27 and Pen-strep (Fisher Science). Cells were spiked with 20 ng/ml EGF and 20ng/ml FGF (EMD Millipore) every other day. To maintain high transduction efficiency of the GB3-RFP cell line, blasticidin (2 ug/ml) was added to cell culture media every time cells were passaged. Use of GB3 cells was discontinued after the cells reached passage 30.

2.2.3 Formation of Vascular layer:

HUVECs were used to create vasculogenesis in our microfluidic device by suspension in

a fibrin solution. Briefly, HUVECs at 70 – 80% confluency were dissociated from tissue culture flasks using trypsin-EDTA and centrifuged at 1200 RPM for 5 minutes. The cells were then counted and resuspended in fresh EGM-2 media. To make the fibrinogen solution, 5mg/ml bovine fibrinogen (Sigma-Aldrich) was dissolved in Dulbecco's phosphate buffered saline (DPBS, Gibco). Afterwards, bovine thrombin (Sigma-Aldrich) was dissolved in DPBS to form a 4 U/ml thrombin solution. The fibrinogen and thrombin solutions were stored at -20C after filter sterilization (Denville Scientific) to prevent denaturing.

To make the fibrin hydrogel have a final cell density of 20 million cells/ml, equal portions of fibrinogen, HUVEC cell suspension and thrombin were mixed in a 1:1:1 ratio respectively. The fibrin solution was immediately injected into the vascular region of the device. All solutions were kept on ice to avoid premature polymerization of the fibrin solution. After immediate injection into the vascular layer, the devices were incubated for 10 minutes at 37C to encourage fibrin polymerization and flipped every minute to ensure even distribution of the cells in the 3D matrix. Next, EGM-2 supplemented with extra 50 ng/ml Vascular endothelial growth factor (VEGF, Millipore) was added to the media channels of the devices.

The devices were then placed in a petri dish containing DI water and then kept in the incubator at standard conditions (37C, 5% CO2) for 72 hours. The essence of the DI water was to provide humidity to prevent the media in the devices from drying up, since they were in very low amounts. Cell culture media was exchanged every 24 hours throughout vasculogenesis.

2.2.4 Injection of GB3 cells and Normal Human Astrocytes (NHA):

To form the tumor model in the devices, NHA and GB3 cells were injected into the tumor and stroma regions of the devices. Specifically, GB3 spheroids were dissociated using Accutase (Invitrogen) and centrifuged. The cell suspension was mixed with equal portions of Matrigel® (Corning) in a 1:1 ratio to form a final cell density of 15 million cells/ml. The hydrogel was then immediately injected into the tumor region of the device and allowed to polymerize at 37 degrees Celsius for 3 minutes. Following this, pure Matrigel® was injected into the stroma region for monoculture and coculture conditions. Devices were allowed to polymerize at 37 degrees Celsius for 5 minutes, after which Neural Stem Cell (NSC) media was added to the media channels.

Devices were then kept in the incubator under standard conditions for 72 hours.

For coculture with astrocyte, and triculture conditions, normal human astrocytes (NHA) cells were dissociated with trypsin-EDTA, centrifuged and directly suspended in pure Matrigel® in a 1:1 ratio to form a final cell density of 3 million cells/ml. The hydrogel solution was then immediately injected into the stroma regions of the devices very carefully to avoid leakage into the vascular regions. The hydrogel was allowed to polymerize at 37 degrees Celsius for 7 minutes. Next, NSC medium was added to the media channels, and devices were kept in the incubator for 72 hours under standard conditions. Cell culture media was changed every 24 hours in all conditions.

2.2.5 Immunofluorescence staining:

For proliferation and stemness studies through immunofluorescence (IF), microfluidic devices were fixed with warmed 4% paraformaldehyde (PFA) by removing the cell culture medium and replacing it with PFA. Devices were incubated at room temperature (RT) for 30 minutes, after which devices were washed twice with PBS-glycine (100mM glycine in PBS) and once with PBS-Tween (0.05% (v/v) Tween-20 in PBS) for 10 minutes each at RT to permeabilize the cells. To block the cells, immunofluorescence (IF) buffer (0.2% (v/v) Triton X-100, 0.1% (v/v) BSA (radioimmunoassay grade), 0.05% Tween 20, 7.7mM NaN3 in PBS) was added to the outlets of the devices and negative pressure was applied to the inlets to create flow. The devices were then incubated at RT for 1 hour. Following this, 10% goat serum (GS) in PBS tween was added to the devices in similar fashion, and devices were incubated for an additional hour to prevent nonspecific binding of antibodies.

Next, the primary antibodies of interest were diluted in goat serum and added to the devices. The samples were then placed in petri dishes and taped with parafilm to prevent evaporation. The devices were kept at 4C overnight to ensure thorough targeted binding of antibodies. After exposure to primary antibodies, devices were washed 3 times each at 20 minutes intervals with IF buffer at RT. Alexa-conjugated species matching secondary antibodies diluted in PBS-Tween were centrifuged at 14k RPM for 10 minutes and added to the devices. Devices were incubated at RT for 45 – 3 hours in the dark. The devices were then washed 3 – 5 times in PBS-Tween at 20-minute intervals each, after which 4'6-diamidino-2-phenylindole (DAPI, Invitrogen) at a

1:1000 dilution was added to the devices and kept at 4C overnight. Next, devices were finally washed 5 times at 10- minute intervals in PBS-Tween.

The antibodies used were Human Nestin (1:200, Anti-Human Nestin (10C2) Mouse NB300-266 (Novus Biologicals)), anti-GFAP(1:400, (GA5) Mouse mAb #3670 (Cell Signaling Technologies)) anti-SOX2 (1:400, (D6D9) XP Rabbit mAb #3579, Cell Signaling Technologies), anti-CD44 (1:400, (156-3C11) Mouse mAb #3570 (Cell Signaling Technologies)), anti-AQP4(1:100, (D1F8E) XP Rabbit mAb #59678 (Cell Signaling Technologies)), anti-Ki-67 Rabbit ab15580 (Abcam)(1:1000), mouse CD31 (10 ug/ml, P2B1, Developmental Studies Hybridoma Bank, DHSB).

2.2.6 Viability Assay:

To determine the viability of cells in the vascular layer, a Live/Dead Assay kit (life Technologies) was used. Calcein AM (CI) and Ethidium homodimer (EthD) were added to the devices at the end of the experiments. Briefly, the devices were carefully washed twice in PBS-Tween, after which a dye solution comprising 5 µ l CI, 20 µ l EthD and 10ml warm PBS was vortexed and added to the devices. The devices were then incubated at RT for 45 minutes. The dye solution was then replaced with PBS to prevent non-specific staining and fluorescent tile images were taken with the 10x magnification of the Zeiss Axio Observer microscope as described below. To calculate the survival percentage of cells, the total number of live and dead cells were each counted, and the total number of viable cells was calculated by subtracting the number of dead cells from the total number of cells. Quantification and analysis of the data was performed in GraphPad prism, and the results were reported as average standard deviation.

2.2.7 Imaging and Statistical Analysis;

Phase contrast and fluorescent images were captured with the Zeiss Axio Observer Z1 with Apotome2 (Zeiss) at 10x, 20x and 40x. 10x Phase contrast images were uploaded into the NIH ImageJ software and stitched, while fluorescent images were processed in both ImageJ and the Zen Pro imaging software. For live/dead assays, the following method was used, and a student's t-test was used to analyze the data in GraphPad prism software. At least three independent experiments (n>3) were conducted for each assay, with 2-3 technical replicates each.

2.3 RESULTS

2.3.1 Device optimization and Vasculogenesis;

Based on a previous design template provided by Truong *et al*, the microfluidic device used for this study was developed (D. Truong et al.). Specifically, it was improved to tolerate injection of astrocytes into the stroma layer without leakage of cell to the vascular layer. It consisted of three concentric cell culture regions, namely the vascular layer, stroma layer and tumor layer **(Figure 2.2 b)**. It also had surrounding media channels for holding media, as well as inlets and outlets for injecting cells and media. All channels in the chip had a height of 200 μm, and hexagonal microposts evenly spaced at 100 μm delineated every channel and allowed the hydrogels to attach and polymerize. The vascular layer had a diameter of 500 μm, while the stroma layer had a diameter of 750 μm. Furthermore, the shape of the microposts were modified from the old trapezoidal shape to a hexagonal shape **(Figure 2.2 c)**. This was made to allow the channels enough shear stress to contain the hydrogel being injected between the vascular and tumor layers without leaking into the vascular layers.

Although the devices were surface treated to increase hydrophobicity, the hexagonal shape of the microposts were still required to help keep the hydrogels in their specific channels. The channels in the microfluidic device were bound by transparent glass slides that permitted real time imaging of intercellular interactions. To ensure that the cells were evenly encapsulated in the ECM and not attached to the glass slides, we employed a technique known as flipping while forming the vascular layer. This involved turning the chip over every minute during fibrin polymerization to ensure even distribution of cells in the matrix and allow for formation of properly interconnected 3D vessels.

Also, we supplemented the cell culture media with VEGF, since VEGF has been shown to promote vascular formation in the TME (Taylor et al.). We monitored the formation of the vascular layer over the course of 72 hours by taking phase contrast images every 24 hours **(Figure 2.3 a),** as well as staining for actin at the end of the 72-hour experimental period **(Figure 2.3 b)**. We confirmed that the formed vessels had similar morphology with our previous studies (48 ± 9 um) (D. Truong et al.) by measuring the diameter of the vessels across five different fields of view.

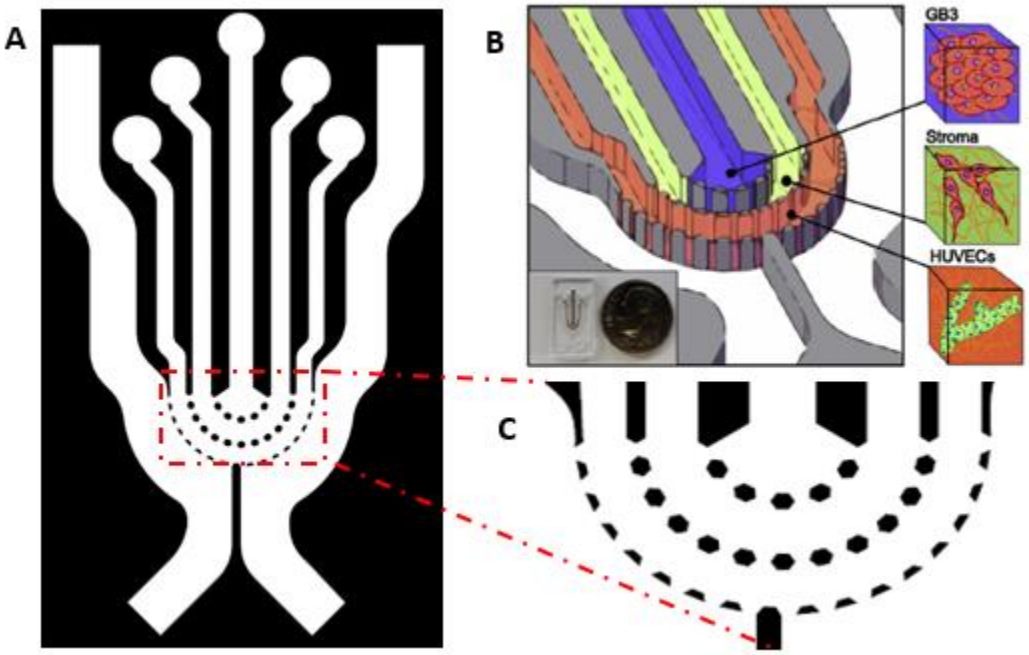

Figure 2.2: Schematic showing engineered microfluidic device for glioma stem cell invasion studies **(a)** Schematic of microfluid device showing media channels and cell culture regions **(b)** schematic of microfluidic device showing specific cell culture regions; blue region - tumor layer for glioma stem cell culture; yellow region - stroma layer for astrocyte cell culture; orange region - vascular layer for endothelial cell culture and formation of vascular layer. Adapted from Truong et al. with permission from Biomaterials (2018) (Truong et al. 2018). **(c)** Zoomed in image showing cell culture region of microfluidic device. Hexagonal posts employed to reduce leakage of hydrogel during injection.

2.3.2 Establishment of vascular network

Following device fabrication, sterilization and surface treatment, a cell matrix solution was made by mixing equal portions of fibrinogen, HUVEC cell suspension and thrombin. To determine the appropriate amounts of media to resuspend HUVECs before embedding in fibrin matrix, we divided the total number of HUVECs counted after trypsinization by a 60 million cell/ml density. After incorporating the cell matrix solution into the vascular layer, EGM-2 media supplemented with 50ng of VEGF was injected, and the cells were allowed to develop and mature over a course of 72 hours. After formation of the vascular layer, we sought to investigate the morphology of the spontaneously formed vessels. By staining for CD31 and Actin **(Figure 2.3 b),** we observed interconnected vessels with diameters consistent with our previous studies (D. Truong et al.).

Since the GBM TME has been associated with leaky vessels, we sought to investigate the morphology of our spontaneously formed vessels in the triculture condition after insertion of GB3 cells and astrocytes **(Figure 2.3 b).**

2.3.3 Establishment of monoculture, coculture and triculture platforms

Briefly, GB3 patient derived GSCs were dissociated and embedded in a Matrigel® matrix at a cell density of 15 million cells/ml. The cell-matrix solution was then incorporated into the tumor layer of the microfluidic device and allowed to polymerize for three minutes. To form the monoculture condition, the GB3 cell-matrix solution was injected into a fresh device, after which NSC media was added to the media channel **(Figure 2.4 b)**. To form the coculture with vasculature condition, the GB3 cell-matrix solution was added to the tumor layer of devices which had already formed vascular layers. After allowing the matrix to polymerize for 3 minutes, pure Matrigel® was injected into the stroma layer of the device, after which NSC media was introduced through the inlets of the media channels **(Figure 2.4 b)**.

To form the coculture with astrocytes condition, the GB3 cell matrix solution was incorporated into a fresh device and allowed to polymerize for three minutes. Following polymerization, astrocytes embedded in a Matrigel® matrix at a 3 million cells/ml density and were introduced into the stroma layer and allowed to polymerize for five minutes, after which NSC media was introduced into the media channels. Finally, to form the triculture condition, the GB3 cell-matrix solution was incorporated into devices that had already formed vascular layers. After polymerization, an astrocyte cell-matrix solution was injected into the stroma layer of the devices and allowed to polymerize for five minutes, after which media was added to the media channels **(Figure 2.4 b)**. All devices were then kept under standard conditions and observed over a 72-hour period.

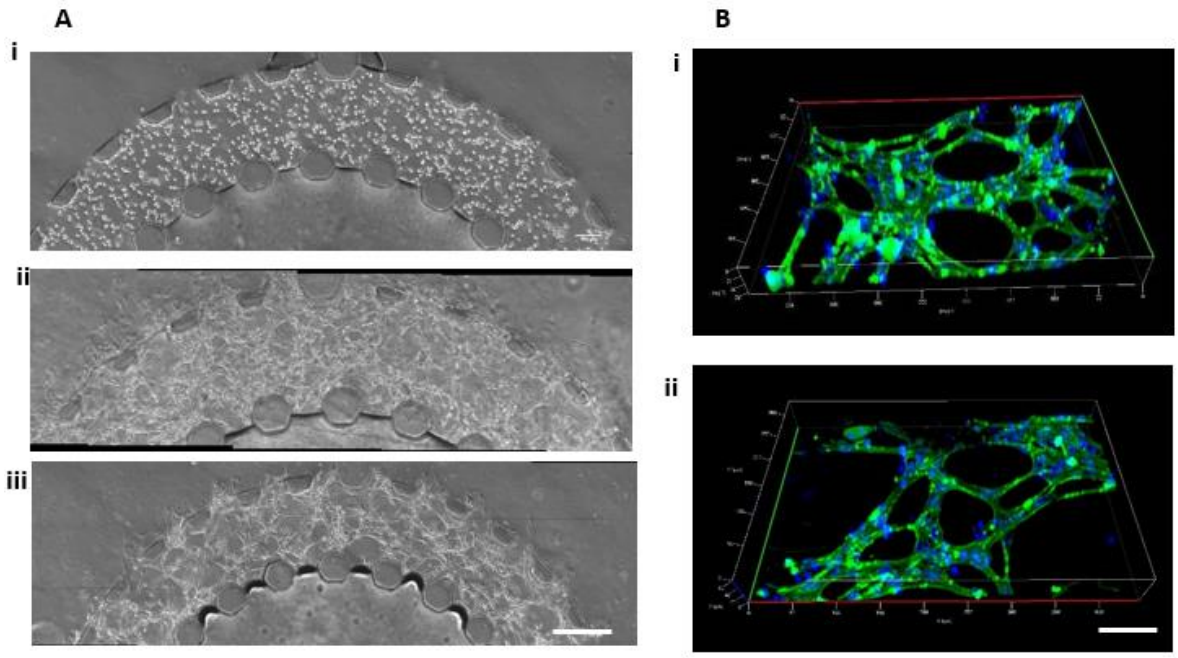

Figure 2.3: Formation of vascular layer in engineered microfluidic model **(a) (i)** Phase contrast image showing formation vascular layer of microfluidic device with endothelial cells embedded in fibrin matrix **(ii)** Phase contrast image of vasculature formation 24 hours post-injection **(iii)** Phase contrast image showing formed vascular layer 72 hours post-injection. Scale bar; 100um **(b)** CD-31 fluorescent image confirming morphology of formed vascular layer within microfluidic device Scale bar: 100um. (green: actin, blue: DAPI).

We confirmed that the vascular layer formed in the triculture condition **(Figure 2.4)** indeed had a disrupted morphology at day 6 as compared to the other experimental conditions **(Figure 2.3 b)**. To avoid attributing the disrupted morphology of the vessels to GSCs solely, we also investigated their morphology at day 6 by switching the media from EGM-2 + VEGF after 72 hours to pure NSC media. This was to determine whether the media composition had presented a contributory factor to the morphological differences of the vascular layer observed.

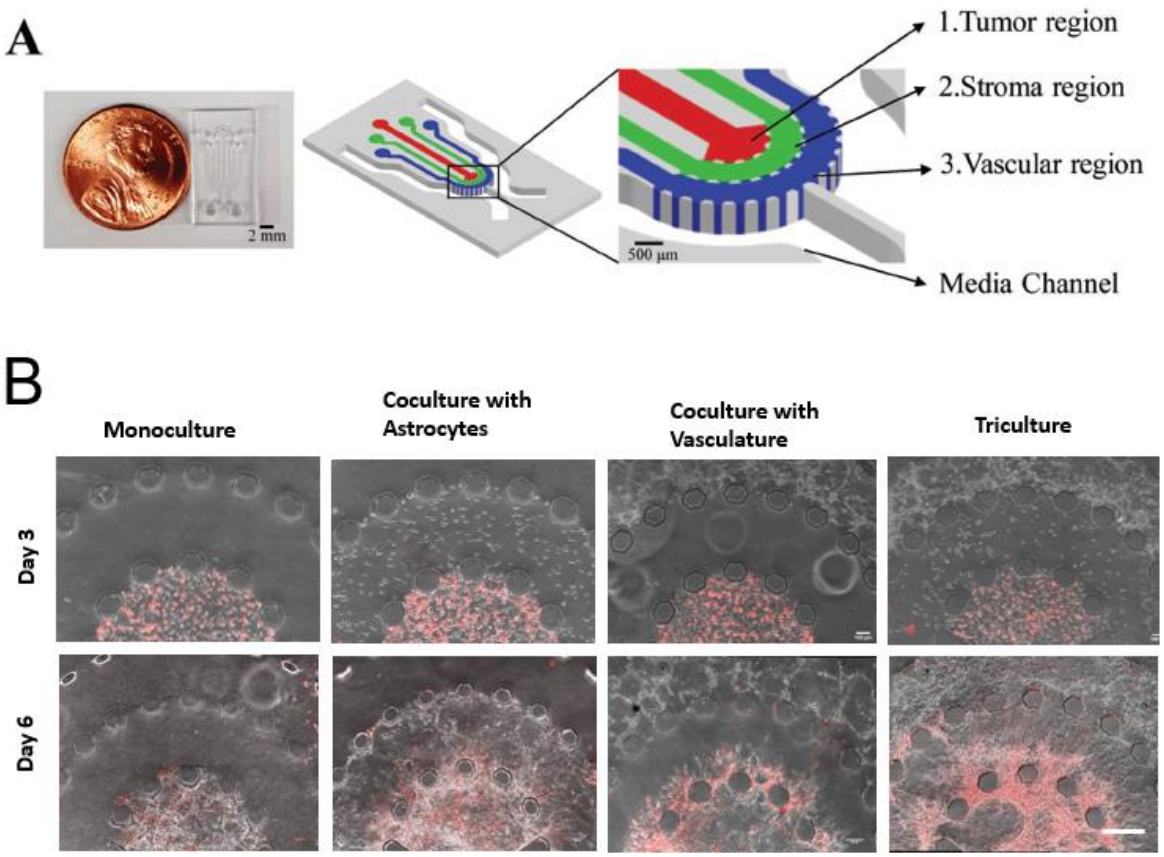

Figure 2.4: Establishment of monoculture, cocultures and triculture conditions in microfluidic device **(a)** Schematic of microfluidic device showing different channels of the device. Adapted with permission from Advanced Healthcare Materials (copyright 2017) (Nagaraju et al.) **(b)** Phase contrast images showing four different experimental conditions established for glioma stem cell invasion studies. Red indicating GSCs. Scale bar; 100um.

We also sought to determine whether the presence of the astrocytes influenced the viability of the vasculature. Therefore, we performed a viability test at day 3 and day 6 of our experimental conditions **(Figure 2.3 a)**. As shown in figure 2.3a iii, we observed a very high cell survival (>95%) across all experimental conditions. This proved that the presence of the astrocytes did not negatively impact the viability of the vascular layer.

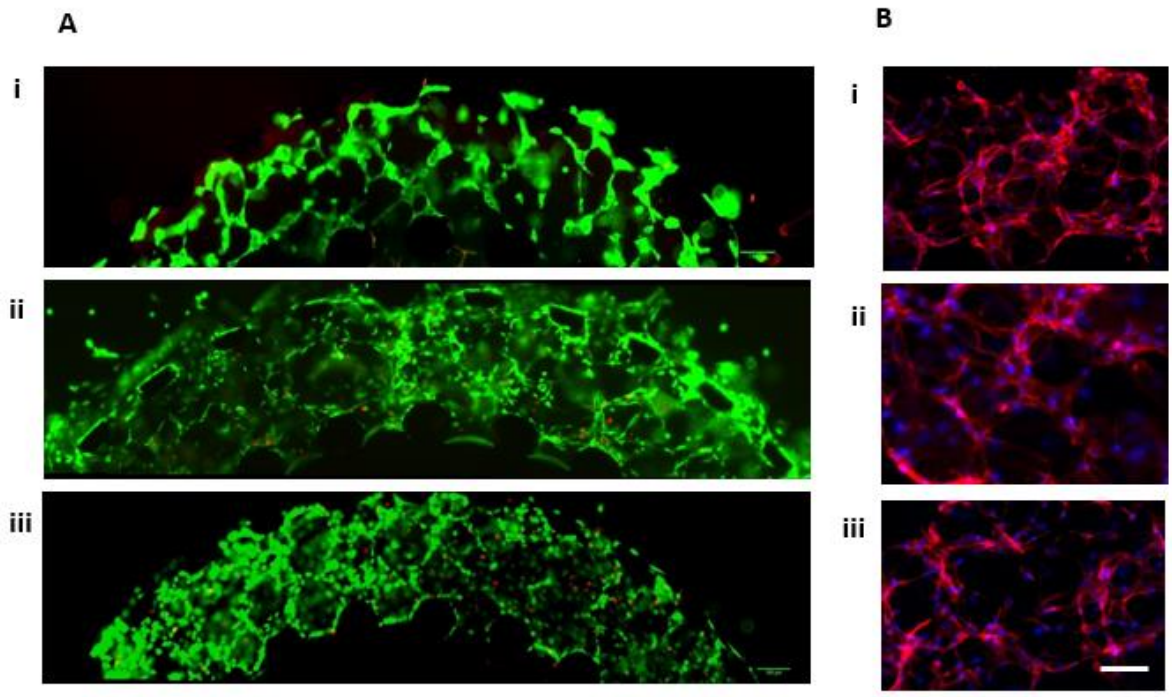

Figure 2.5: Viability and morphology of Vascular layer within microfluidic device **(a) (i)** Live/dead fluorescence image of vascular layer at day 3 before GSC injection. **(ii)** Live/dead fluorescence image of vascular lay at day 6 in NSC media without glioma stem cells in tumor layer **(iii)** Live/dead fluorescence image of vascular layer at day 6 in NSC media with GSC and astrocytes in tumor layer and stroma layer respectively. Red: Dead cells, Green: Live cells **(b) (i)** CD31 staining of vascular layer at day 3 before GSC incorporation **(ii)** CD-31 staining of vascular layer at day 6 in NSC media without GSC in tumor layer **(iii)** CD-31 staining of vascular layer at day 6 with GSC and astrocytes present in tumor and stroma layers respectively. Red; CD-31, Blue: DAPI. Scale bar: 50um.

2.4 DISCUSSION

In this study, we presented an improved design of our microfluidic platform that allowed for the culture of three different cell types simultaneously. Although previous studies have introduced microfluidic devices to investigate GSCs invasion, they still lack significant cues present in the perivascular niche of the tumor microenvironment. Therefore, the advantage of our device was the fact that we were able to model a 3D vascular layer, as well as the presence of stromal cells which are abundant in the TME and are responsible for maintaining homeostasis. Also, by introducing stromal cells between the vascular layer and the tumor layer, we created a greater impedance of the GSCs to nutrients, thereby creating a hypoxic environment.

Our model therefore composed of various biomechanical and signaling cues present in the

perivascular niche and was therefore an adequate platform to study GSC invasion *in vitro.* To study GSC invasion, we initially formed a vascular layer in our microfluidic chips and allowed them to mature for 72 hours after which we investigated their morphology by staining for CD31 and actin. Specifically, we investigated the morphology of the formed vascular layer under three different conditions (Day 3, Day 6 in NSC, Day 6 in NSC + GB3 cells). We hypothesize that the reason for the disrupted vascular layer at day 6 was likely due to the change in media composition after 72 hours and most importantly the presence of the GB3 cells, because the vascular layer at day 3 appeared to be more connected and distinct, as compared to the other conditions. This is consistent with previous findings where leaky vessels have been attributed to the increased concentration of VEGF in the TME and have been accepted as a hallmark of cancer (Calabrese et al.).

Astrocytes are evidently present in the perivascular niche in larger quantities and contribute to the invasiveness of the tumor (Guan et al.) (Henrik Heiland et al.) (Hambardzumyan & Bergers). We sought to recapitulate this cue by introducing astrocytes into the stroma layer of the device. Although we intended to make sure that there were just enough populations of astrocytes, we also had to keep in mind the physical barrier it presented to migrating GB3 cells. Therefore, we initially begun our astrocyte cell density optimization at 15 million cells/ml. Using this cell density, we realized that the astrocytes posed a huge physical barrier to the GB3 cells and inhibited migration which was inconsistent with previous results. Therefore, we further optimized the cell density and finally selected an astrocyte cell density of 3 million cells/ml. This cell density was optimal because it allowed the GB3 cells enough space to migrate while simultaneously proliferating to produce an adequate astrocytic presence.

To establish a well thought out experiment, we introduced four experimental conditions for subsequent experiments **(Figure 2.1, 2.4).** These conditions allow us to properly investigate the contribution of astrocytes to GB3 invasion, stemness and proliferation which are further discussed in chapter 3.

CHAPTER 3

ESTABLISHMENT OF 3D MICROFLUIDIC PLATFORM TO STUDY MIGRATION, PROLIFERATION AND STEMNESS OF GLIOMA STEM CELLS (GSCs)

3.1 INTRODUCTION

Glioma stem cells (GSCs) have been shown to be the driving forces behind tumor initiation, tumor progression and tumor recurrence. An estimated 20% of all tumors treated with chemotherapy return within a period of 2-5 years (Omuro & DeAngelis). This is because the perivascular niche acts as an optimum environment, supplying the GSCs with growth factors and increasing their chemoresistance (Hanif et al.). Within the perivascular niche, glial cells like microglia and astrocytes have been shown to contribute immensely to tumor progression and aggressiveness, however, their mechanism of action is not fully understood.

On normal occasions, astrocytes are responsible for maintaining homeostasis in the brain microenvironment (Matias et al.). However, when an injury occurs, they modify their activities to prevent further injury (Fidoamore et al.). For tumor cells, the glial cells do not recognize their presence as a threat, therefore they do not fight off the tumor, however, they begin to serve as the links between the tumor microenvironment and the vascular region of the brain (Matias et al.). In previous studies, scientists discovered that astrocytes create Gap Junctional Communication (GJC) between themselves and the tumor (Lin et al.). It was proven that these gap junctional communications were also responsible for providing the GSCs with chemoresistance and thereby increasing their survival (X. Wang et al.) (Lin et al.).

Although much is known about microglia and their influence on GSC invasion, very little is known about that of astrocytes. In this study, we developed a microfluidic device that permitted the triculture of three different cell types in the perivascular niche. This model presented herein has a very high physiological relevance due to the various microenvironmental cues incorporated into the device. HUVECs were used to form a spontaneous vascular layer as demonstrated in the previous chapter, and patient derived GSCs were embedded into Matrigel® and introduced into a tumor region. Normal human astrocytes (NHA) were also embedded in a 3D matrix and introduced into

the stroma layer of the microfluidic platform. By studying the invasion, proliferation and stemness of the glioma stem cells, we gained a better understanding of the influence of the components in the perivascular niche on GSCs.

3.2 MATERIALS AND METHODS

3.2.1 Microfluidic device fabrication:

Microfluidic devices used for all experiments were fabricated according to the protocol described in section 2.2.1 above.

3.2.2 Cell culture:

All patient samples and cells used for the experiments were cultured according to the protocol described in section 2.2.2 above.

3.2.3 3D cell injection:

To form the 3D vascular-tumor model, the protocol described in 3.2.4 was followed. Vasculogenesis was formed in 72 hours, after which GB3 cells and astrocytes were injected. After GB3 and NHA injection, the cell culture medium was changed from EGM-2 (supplemented with extra VEGF) to NSC media for the rest of the assay (72 hours). Cell culture media was changed every 24 hours, and devices were kept humidified to avoid evaporation of media from the devices.

3.2.4 Migration studies:

Migration of GB3 cells were monitored over a 72-hour period. To quantify migration in the various experimental conditions, lines were drawn from the middle of the hexagonal posts to the tip of the GB3 cell extension. 15 measurements were taken per device across 5 fields of view (FOV) in ImageJ.

3.2.5 EdU assay:

For proliferation studies, a Click-iT Plus EdU Imaging kit (Life technologies) was used. The kit composed of 5-ethynyl-2'-deoxyuridine (EdU), Alexa Fluor picolyl azide, Dimethylsulfoxide (DMSO), Click-iT EdU reaction buffer, copper protectant, Click-iT EdU buffer additive and Hoeschst 33342. Briefly, all vials were warmed to room temperature, and a 10mM solution of EdU was prepared by adding 2ml DMSO to the EdU. All remaining solutions were stored at -20C. a working

solution of 1X click-iT EdU reaction buffer was prepared by dissolving in DI water. To make smaller amounts of the 1X Click-It EdU reaction buffer, the initial volume was diluted 10X in DI water, and remaining solutions were stored at 2-8C. To make a 10x stock solution of the Click-iT EdU buffer additive, 2mL DI water was added to the vial and mixed until it was fully dissolved.

To label samples with EdU, a 2X working solution of EdU was prepared in NSC medium with a 10uM concentration. The EdU solution was prewarmed and added to an equal volume of NSC media, after which the resulting solution was added to all samples and incubated under standard conditions for 24 hours. After exposure to EdU solution, the media in the devices was replaced with 3.7% PFA in PBS and incubated at RT for 30 minutes. All samples were then washed twice in 3% Bovine Serum Albumin (BSA) in PBS for 10-minute intervals each after which i0.5% Triton X-100 in PBS was added to the samples and incubated for 30 minutes at RT.

After permeabilization, devices were washed twice in 3% BSA for 10 minutes each, and then a 500uL Click-iT Plus reaction cocktail was prepared and added to all devices. The devices were incubated at RT for 30 minutes, after which they were washed once with 3% BSA for 10 minutes. Following this, all samples were counterstained with DAPI by diluting DAPI in PBS-tween (1:1000) and adding to devices for 3 hours. Following this, all devices were washed 3 – 5 times in PBS-tween, and 20X fluorescent images were captured using the Zeiss microscope.

3.2.6 Immunofluorescence staining:

All antibodies were stained according to the protocol described in section 2.3.5.

3.2.7 Fibrinolysis:

To extract cells from the 3D matrix after the experiments, it was necessary to digest the ECM matrix. Devices were washed once with PBS. Next, Nattokinase (NSKD, Japan Bio Science Ltd) was dissolved in PBS containing EDTA and added to the media channels of the devices. Devices were then incubated for 1 -1.5hrs, after which the hydrogels were mechanically dissociated by slightly pipetting up and down for 30 seconds. The hydrogel solution was then retrieved from the devices and centrifuged.

3.2.8 Imaging and Data Analysis;

Phase contrast images were captured using the Zen Pro microscope and imaging software. Multiple 10x images were taken and stitched together in ImageJ. All measurements were taken in ImageJ and statistical analysis was performed in GraphPad Prism. For migration analysis, a student's t-test with Wilcoxon analysis was used. For migration and stemness analysis, an unpaired t-test was used. Values were obtained from at least three independent experiments (n>3) with 3 – 4 technical replicates each, and the data was expressed as an average standard deviation. Statistical significance was established at $p<0.05$.

3.3 RESULTS

3.3.1 Migration of GSCs in established experimental conditions:

Under the stated conditions (monoculture, coculture with astrocytes, coculture with vasculature and triculture), migration distance was measured by drawing a line between the center of the hexagonal microposts and the tip of the patient derived GB3 cell extensions. Specifically, phase contrast images were captured every 24 hours to monitor the migration of the GB3 cancer cells. By day 1, astrocytes were seen to have spread, while GB3 cells had started to invade the stroma layer in triculture and coculture conditions **(Figure 3.1 a).** By day 3, significant migration of GB3 cells were observed in all conditions but the monoculture condition **(Figure 3.1 b)**. The stroma layer was also packed with astrocytes which had spread and proliferated, and consequently created migration tracts. This phenomenon has been described in the brain tumor microenvironment and has been hypothesized to increase migration speed of GB3 cells (Matias et al.).

Notably, we observed increased migration in the coculture with astrocyte condition and not in the monoculture condition. We also observed a difference in the morphology of the migrating cells across the experimental conditions. In the conditions that had astrocytes, the extensions of the GB3 cells appeared rather narrow and elongated, while the coculture with vasculature and monoculture conditions had shorter and broader GB3 cell extensions **(Figure 3.2 b)**. We hypothesize that, the astrocytes present an extra mechanical cue due to the packed nature of the stroma, and therefore compels the GB3 cells to squeeze their way through the ECM (M. Wang et

al.). This feature further increases the physiological relevance of our platform, and thus makes our findings more translative for future drug studies.

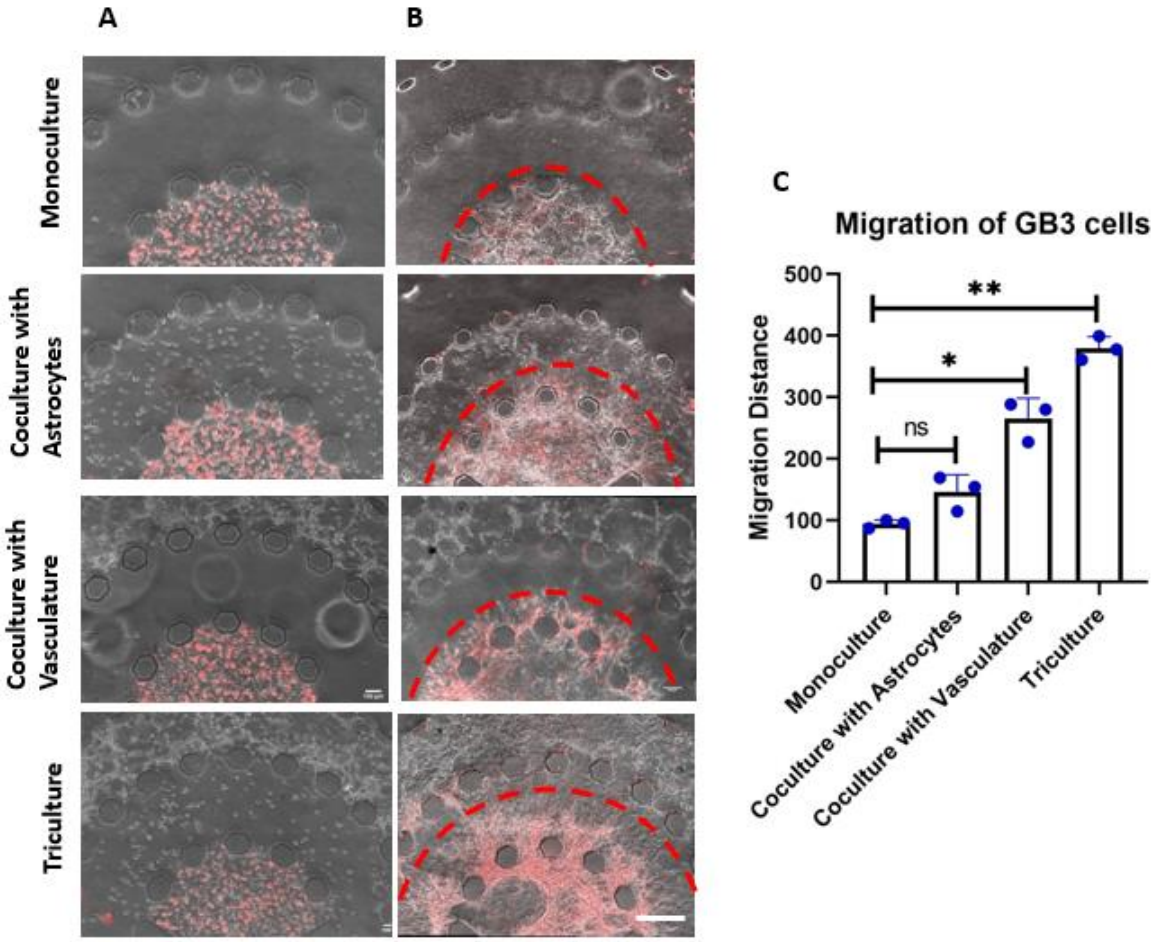

Figure 3.1: Migration of GB3 cells in microfluidic platform **(a)** Phase contrast images showing presence of GB3 cells (red) in tumor layer of microfluidic device with either HUVECs and or NHAs. **(b)** Phase contrast image showing migration of GB3(red) cells across all conditions. Black dashed line representative of average migration distance across all conditions; Scale bar: 100um. **(c)** Quantification of migration distance across four experimental conditions; Blue dots showing distribution of data points. (* denotes $p < 0.05$; Students T-test; n>3 for each dataset).

Similar to our previous publication (D. Truong et al.), the morphology of the invading GB3 cells were studied. We observed that in conditions where astrocytes were present, the GB3 cells possessed thinner extensions as compared to the other conditions. Also, the length of the invading cells appeared to be longer in conditions with astrocytes. We measured the extensions of the GB3 cells in NIH ImageJ software and analyzed them in GraphPad prism. We realized that the presence of the astrocytes in the tumor layer resulted in increased elongation of the GB3 cells **(Figure 3.2b)**

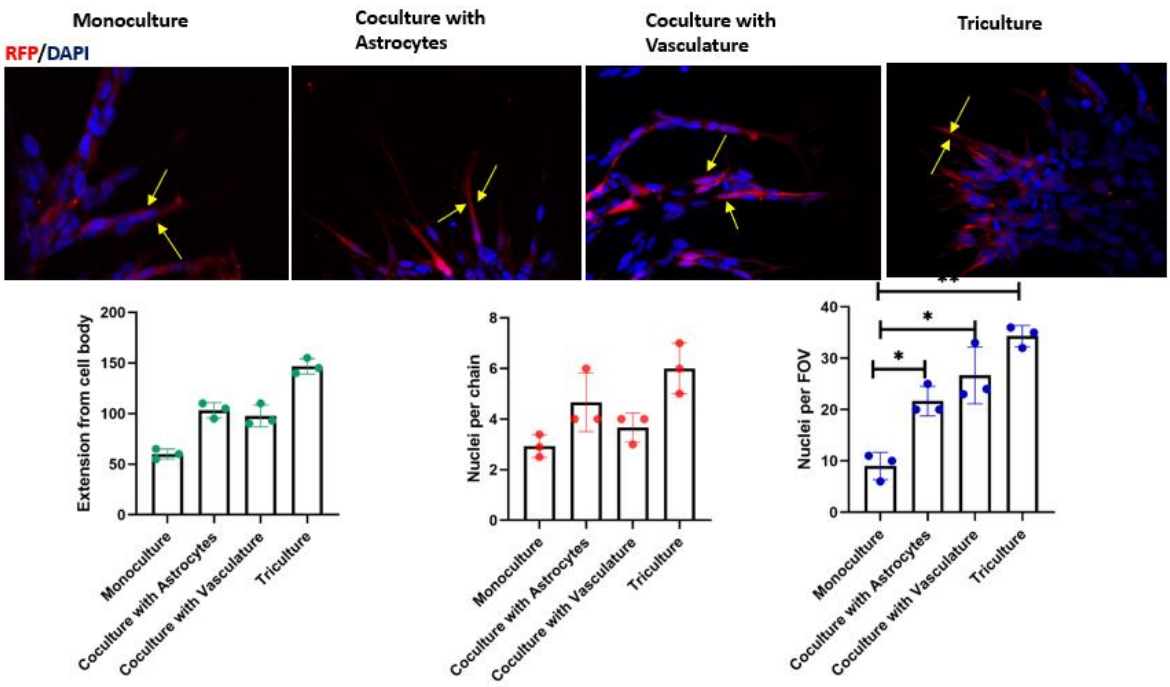

Figure 3.2: Morphology of migrating GB3 cells in stroma layer **(a)**Fluorescent image showing GSC extensions in stroma layer. Red: RFP, Blue: DAPI. Scale bar: 50um **(b)** Quantification of extensions of migrating GB3 cells in stroma layer **(c)** Quantification of density of migrating cells per chain in stroma layer **(d)** Quantification of number of nuclei per field of view of migrating cells. Green, red and blue dots representative of distribution of data points. (* denotes $p < 0.05$; Students T-test; n>3 for each dataset).

Also, the elongation of the GB3 cells in the monoculture and coculture with vasculature conditions were consistent with previous findings (D. Truong et al.). Studying the migration density by counting the number of cells in a select field of view in the stroma layer, and the number of cells in a migrating chain further advised on the morphology of the migrating cells **(Figure 3.2 c)**.

3.3.3 GB3 cell proliferation under established experimental conditions:

We further studied the proliferation of the GSCs under the four different conditions by staining for Ki-67 and additionally pulsing with EdU for 24 hours. After immunostaining the samples with these markers, we measured the proliferation of the GSCs in all the conditions. Specifically, we measured the proliferation of these cells by counting the total number of $DAPI^+$ cells in our selected field of view, and then counting the number of $KI\text{-}67^+/EdU^+$ cells and then dividing this number over the total number of $DAPI^+$ cells. We observed that, the coculture with astrocyte and

triculture conditions expressed higher proliferative markers (EdU and Ki-67) **(Figure 3.3 c, d)**. However, only the triculture condition was significant across the other conditions. We found that the astrocytes also expressed high proliferative markers which indicated that they were proliferating. To confirm the proliferative nature of the GB3 cells in conditions with astrocytes, we captured the fluorescent images with the GB3 cells expressing RFP and processed them in the NIH ImageJ software **(Figure 3.3)**. These results indicated that the GB3 cells indeed maintained their proliferate capacity in monoculture and coculture with vasculature conditions, and that astrocytes promoted proliferation of GB3 cells **(Figure 3.3 c)**. This also confirmed our previous speculation that the migration distance recorded was as a result of migration speed, elongation and proliferation of GB3 cells influenced by the presence of astrocytes.

3.3.4 Stemness of Glioma Stem Cells in 3D platform:

To further validate our findings, we also investigated the stemness of the GSC under our four experimental conditions. Although the phenotype of migrating GB3 cells have been investigated in 2D models (Mathiisen et al.), they have not been investigated in such a complex multi cellular culture platform. In recent studies, Truong *et al* investigated the stemness of patient-derived GB3 cells by staining for Nestin, CD44 and SOX2 (D. Truong et al.). Similar to this, we also sought to investigate the expression of these markers after introduction of astrocytes. We speculated that the presence of astrocytes may influence the fate of the GB3 cells by causing them to differentiate, therefore, we also stained for astrocyte specific differentiation markers including GFAP and AQP4.

To stain for these markers, we first conducted a full experiment including the formation of vasculature, injection of GB3 cells in the tumor layer, and injection of astrocytes for the respective conditions. We monitored the experiment for a total of 6 days, after which we proceeded to stain for the select markers. At the end of the experimental assay (day 6) we fixed our samples in PFA and stained them for select stemness markers.

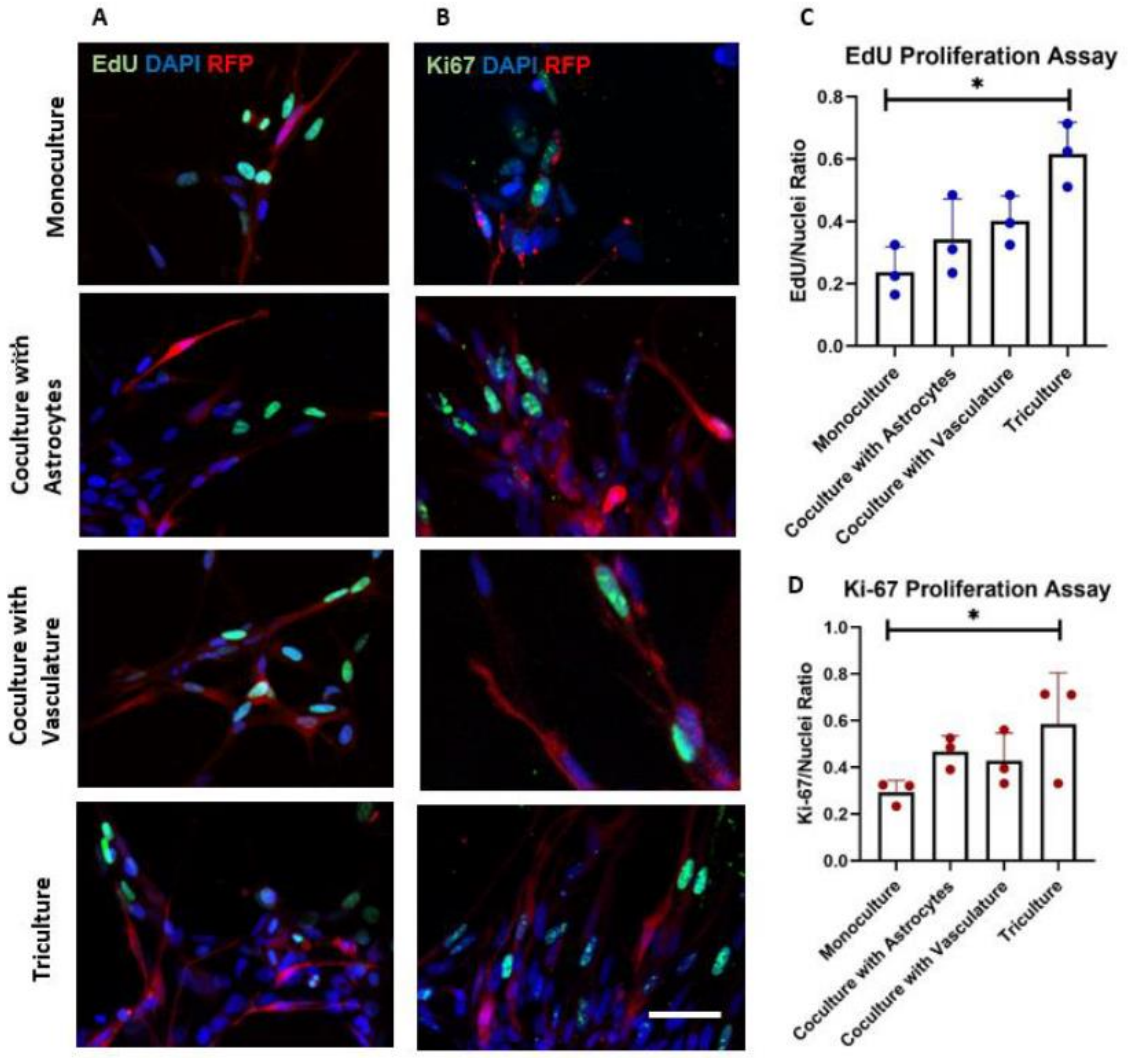

Figure 3.3: Proliferation of GB3 cells **(a)** Immunofluorescent staining of EdU showing proliferation of GSCs in the stroma layer. (Red; RFP, Green; EdU, Blue; DAPI) **(b)** Immunofluorescent staining of Ki-67 proliferation marker of GB3 cells in stroma layer. (Red: RFO, Green: Ki-67, Blue: DAPI) **(c)** Quantification of EdU/Nuclei ratio and Ki-67/Nuclei ratio of all experimental conditions. (* denotes $p < 0.05$; Students T-test; n=3 for each dataset).

All fluorescent images were captured with the Zeiss microscope and Apotome. Specifically, 20X Z-stack images were captured and processed in the NIH ImageJ software. To ensure that we were actually studying the stemness properties of the GB3 cells, we captured all images with GB3 cells expressing RFP. All cells were counterstained with DAPI, and all images were captured in the stroma layer. Nestin, which is a neural stem cell progenitor marker was expressed strongly in the

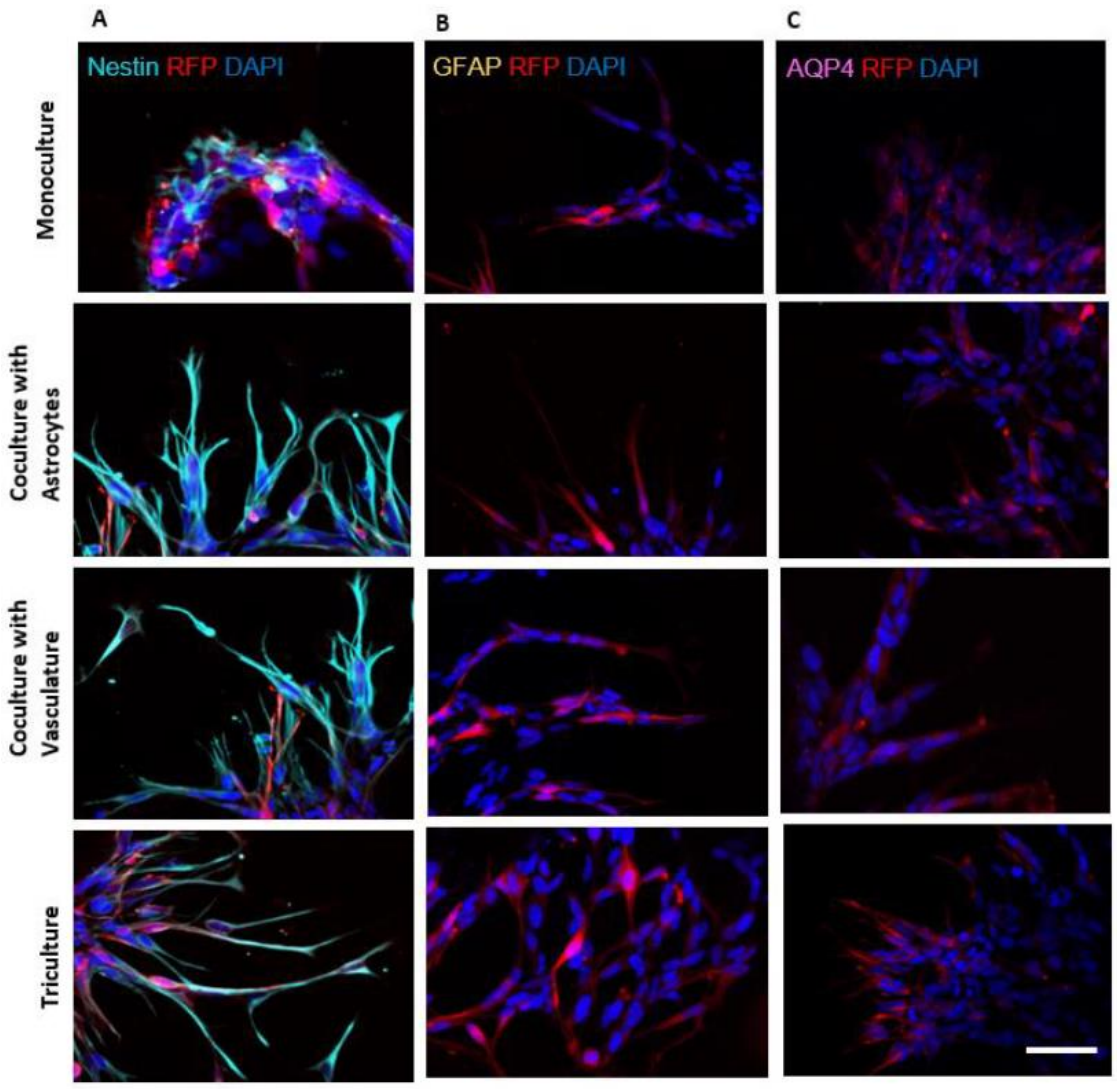

Figure 3.42: Glioma stem cells maintain stem phenotype within microfluidic device **(a)** GSCs express Nestin and **(b)** are negative for GFAP and AQP4 across the four experimental conditions. Scale bar; 50um

GB3 cells in the stroma layer **(Figure 3.4 a)**. However, we did not observe any expression of the astrocytic differentiation markers AQP4 and GFAP in the GSCs **(Figure 3.4 b and c)**. This implied that the GSCs cells maintained their phenotype in the presence of the astrocytes and did not differentiate.

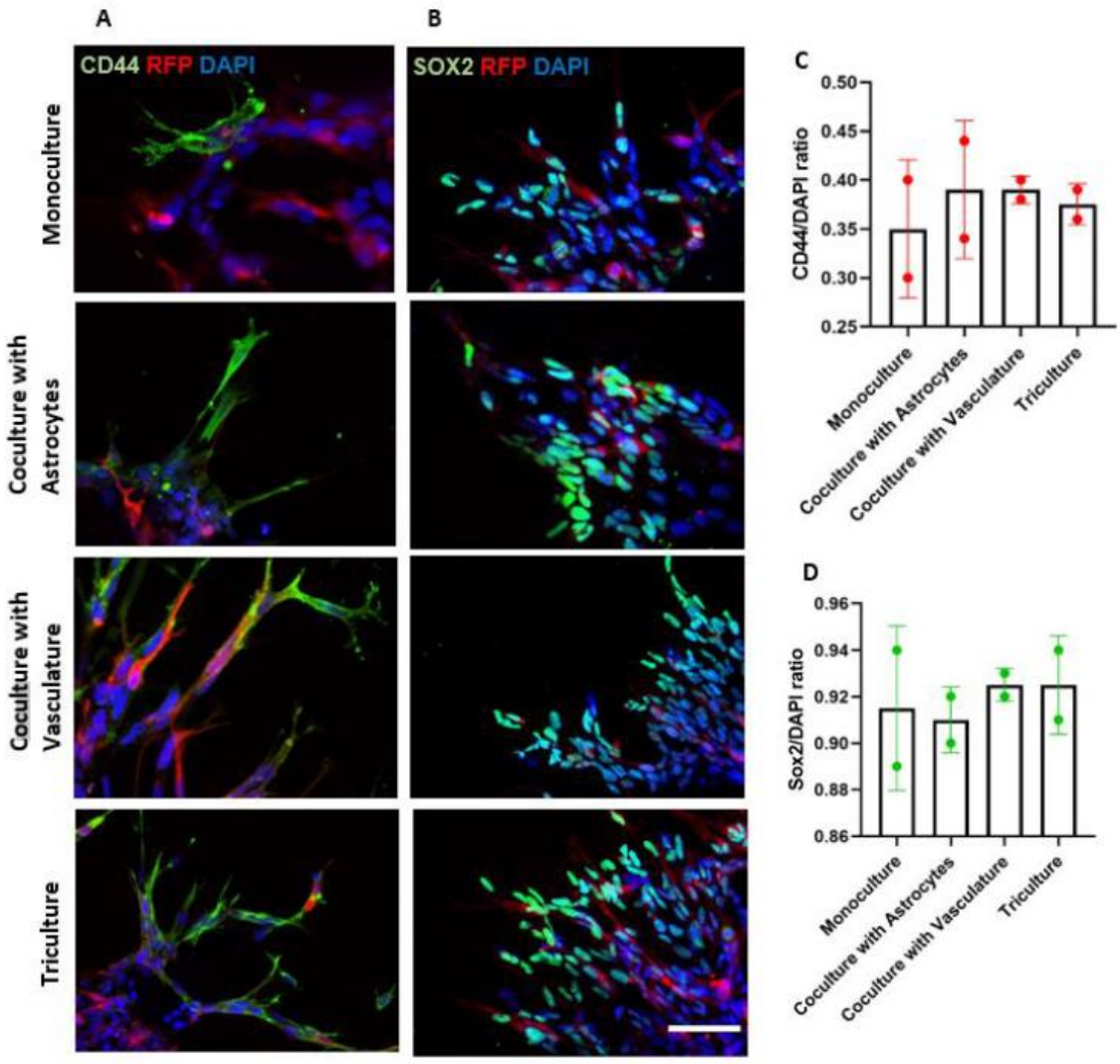

Figure 3: GSCs maintain stemness in 3D microfluidic model **(a and b)** GSCs are positive for CD44 and SOX2 within the stroma layer across all four conditions **(c and d**) Quantification of CD44/Nuclei ratio and SOX2 /Nuclei ratio of all four experimental conditions.

We also observed a low expression of CD44 in GSCs, a cancer stem cell marker expressed in most malignant tumors **(Figure 3.5 a)**. SOX2, which is a self-renewal and pluripotency marker was also expressed in about 90% of GB3 cells in the stroma layer and was expressed most strongly at the tips of the GB3 cell extensions **(Figure 3.5 b)**. We did not observe any expression of SOX2 in the astrocytes in the stroma layer, which proved that they were indeed mature astrocytes.

We therefore hypothesized that the cause of the change in morphology of the migrating GB3 cells in the stroma layer was therefore due to the presence of proliferating astrocytes. Although there were differences in expressions of these select markers across the experimental conditions, we did not observe any significant expression of any of them across the four experimental conditions, consistent with previous studies.

We further intended to examine the expression patterns of the GB3 cells by co-staining specific markers. Specifically, we designed the experiments in such a way to investigate whether the GSCs indeed maintained their phenotype. The experimental design is described in the table below.

Table 1: Staining combinations for stemness studies.

Staining combination	Rationale
CD44 + SOX2	CD44+ SOX2 + cells suggest malignant and stem-like phenotype of GB3 cells
GFAP + Nestin	GFAP + Nestin+ RFP+ cells suggest that these are stem-like cells
GFAP + AQP4	GFAP+ AQP4+ RFP+ cells should indicate that these have differentiated into astrocytes
GFAP + Ki-67	RFP+ GFAP+ Ki67+ cells suggest that these GFAP+ cells can proliferate
Nestin + Ki-67	Are all Nestin+ cells proliferating?

Co-staining Nestin and EdU allowed us to investigate the population of RFP^+ cells that were actually dividing **(Figure 3.6 a)**. We observed significant increase in Ki-67 expression **(Figure 3.3 d)** in the triculture condition and not in other conditions, indicating that the astrocytes influenced the proliferative capacity of the GB3 cells. Co-staining Nestin and EdU also advised us on the population of GB3 cells which had become quiescent neural stem cells. (<5%). Furthermore, co-staining GFAP and Ki-67/EdU advised on whether $GFAP^+$ RFP^+ cells had differentiated into astrocytes or were quiescent neural stem cells. We did not find any $RFP^+GFAP^+Ki\text{-}67^+$ cells **(Figure**

3.6 b), which indicated that the GB3 cells maintained their stemness and proliferative nature. Also, by co-staining for GFAP and Nestin, we confirmed that the GB3 cells indeed exhibited stem-like phenotype **(Figure 3.6 c)**. In addition to the above, we co-stained the two astrocytic markers GFAP and AQP4. This combination advised us on cells that were $GFAP^+$ and $AQP4^+$, since GFAP alone was not a reliable marker for astrocytic differentiation. All GB3 cells were found to be $GFAP^-$ and $AQP4^-$, which indicated that they were not quiescent neural stem cells, neither were they differentiating **(Figure a)**. However, a large population of astrocytes were found to be both $GFAP^+$ and $AQP4^+$, indicating that they were mature astrocytes.

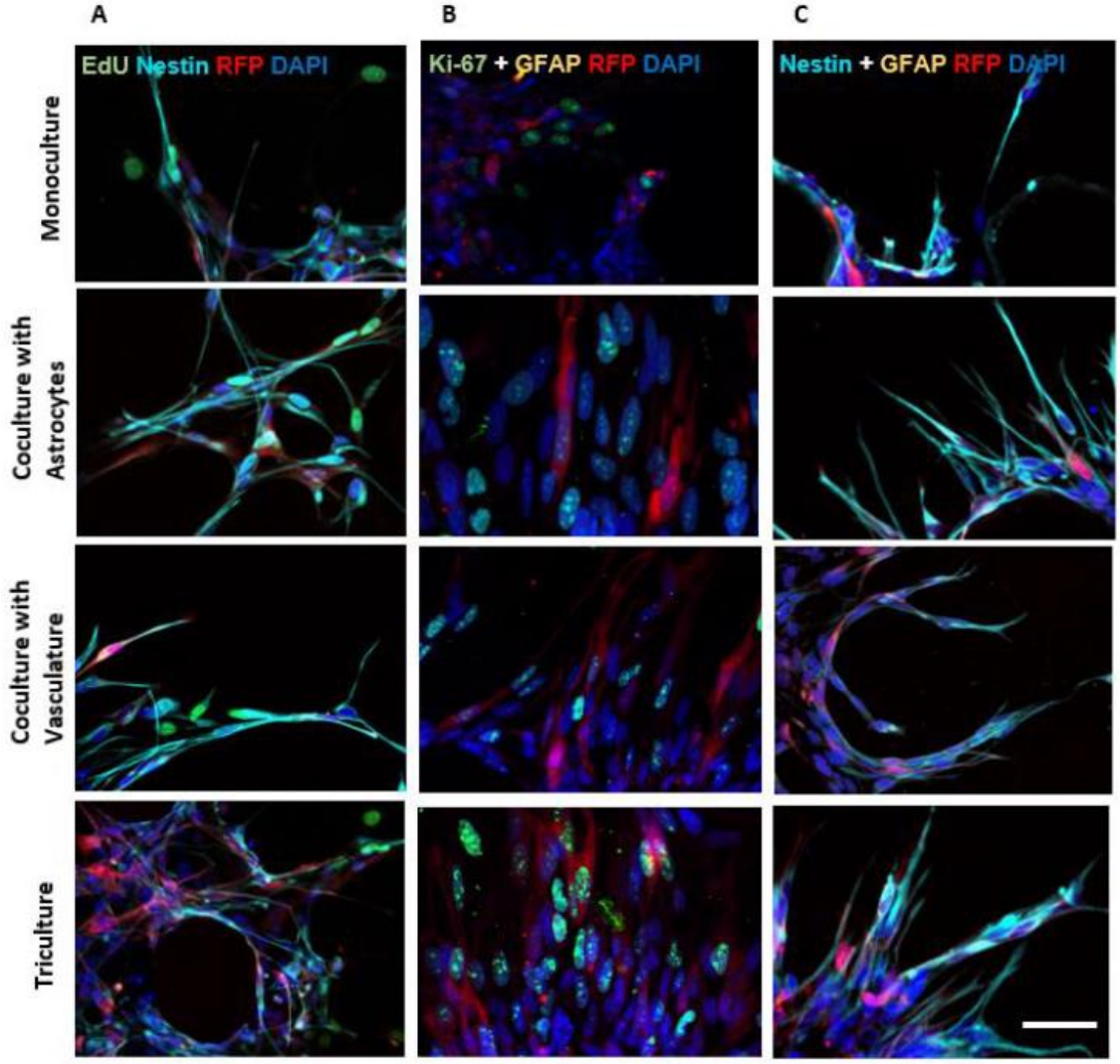

Figure 3.6: Co-stain of stemness markers in stroma layer of GSCs within microfluidic device. **(a)** GSCs express EdU proliferative marker and Nestin **(b)** GSCs express Ki-67 proliferative marker but does not express GFAP in all four experimental conditions **(c)** GSCs are Nestin positive and GFAP negative.

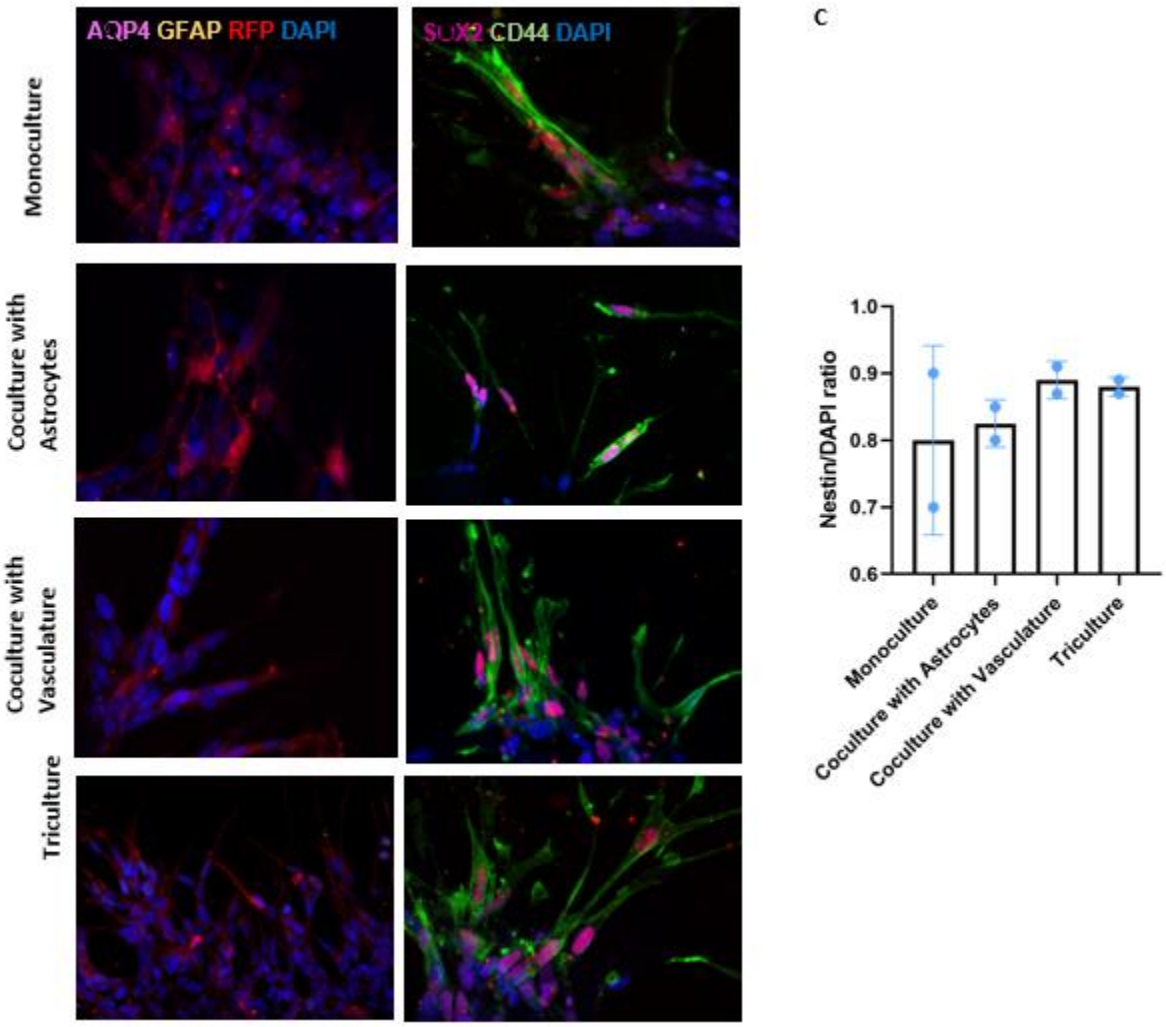

Figure 3.7: Co-stain of stemness markers in microfluidic platform **(a)** GSCs do not express GFAP and AQP4 but **(b)** Express CD44 and SOX2 in stroma layer. **(c)** Quantification of Nestin/Nuclei expression of GSCs in stroma layer of microfluidic device.

Finally, co-staining SOX2 and CD44 allowed us to investigate whether astrocytes were expressing SOX2 or not. All SOX2 $^{+}$ cells were also found to be CD44^{+} which indicated that they were malignant GSCs and not astrocytes **(Figure 3.7 b)**. A majority of the astrocytes expressed both GFAP and Ki-67, which was expected, since astrocytes are glial cells and therefore maintain the ability to proliferate. GB3 cells were also found to be GFAP^{-} which indicated that they were neither changing their fate nor differentiating **(Figure 3.7 b)**.

3.4 Discussion

Various experimental models have investigated the phenotype of dividing GSCs (D. Truong et al.) (C. Wang et al.) (Hira et al.). However, very few studies have shown the phenotype of GSCs under 3D conditions. In our tumor model, GB3 cells were encapsulated in Matrigel® and injected into the tumor layer of our device. Matrigel® is an important ECM component of the GBM TME and is known to be very high in laminin concentration. GB3 cells encapsulated in Matrigel® may therefore have the propensity to differentiate due to the high concentrations of growth factors. Although we switch the medium composition from EGM-2 to NSC to ensure a serum-free model, the growth factors present in both fibrin and Matrigel® can lead to changes in GSC phenotype. Furthermore, the presence of astrocytes may impede and reduce the availability of nutrients to the tumor region and therefore lead to an increase in VEGF due to the formation of a hypoxic environment. This may in turn lead to an increase in tumorigenicity, or a change in GSC phenotype (Infanger et al.).

We sought to investigate the phenotype of the GB3 GSCs across our four experimental conditions. Consistent with previous *in vitro* and *in vivo* studies, all four experimental platforms expressed stem-like malignant tumor properties through the high expression of $Nestin^{+}Ki\text{-}67^{+}CD44^{+}$ cell population. Furthermore, we did not detect any expression of GFAP and AQP4 in the GB3 cells, which indicated that, the presence of astrocytes in the coculture with astrocyte and triculture conditions did not influence the cell fate or stemness of the GB3 cells by causing them to differentiate. Also, by co-staining Nestin and Ki-67, we confirmed that the astrocytes did not cause the GB3 cells to change their fate and become quiescent neural stem cells since about 90% of the cells were both Nestin and Ki-67 positive.

We also sought to investigate the expression of SOX2 and CD44 across our four experimental conditions. By counting the cells that were positive for the cell surface marker CD44, as well as all DAPI and RFP positive cells, we were able to determine whether there were any significant differences across the four experiment groups. Although there were slight differences in CD44 expression across the four experimental groups, none of them had any significance. In a similar fashion, we investigated the expression of SOX2 across the experimental conditions.

Through our analysis, we observed almost 90% expression of SOX2 in the stroma layer across the 4 groups. None of the groups had any significant difference.

Overall, our findings indicate that the astrocytes did not influence the phenotype of the GB3 cells by causing them to dedifferentiate or differentiate, although they promoted invasion and proliferation of GSCs. However, further molecular-level analysis using RNA sequencing that allows us to have a broader view of all the genes involved in GBM tumorigenicity need to be conducted to make a more conclusive judgement. Furthermore, this study proves that GB3 cells maintain their stemness in the perivascular niche, similar to previous studies (D. Truong et al.)

CHAPTER 4

CONCLUSIONS AND FUTURE WORK

4.1 CONCLUSION

Glioblastoma Multiforme (GBM) is the most aggressive form of astrocytoma and has a very low survival rate. Although GBM has no cure, most treatments have focused on eradicating the malignant tumors in the brain, however, due to the presence of a small population of Glioma Stem Cells (GSCs), the tumor recurs within 2 years. The GBM TME has been studied extensively under both 2D and 3D models, however, the influence of stromal cells like astrocytes in tumor progression has not been well studied within microengineered models. In this study, we developed a 3D microfluidic device that permits the triculture of HUVECs, Normal Human Astrocytes, and patient derived GB3 GSCs. Using this microfluidic platform, we investigated the migration, proliferation and phenotypic tendencies of the GSCs under four different experimental conditions, namely, monoculture, coculture with astrocytes, coculture with vasculature and triculture.

Our microfluidic device allowed for real time visualization of migrating GB3 cells over a 72-hour period. Our findings suggested that astrocytes significantly increase the invasion of GSCs and change their morphology by causing them to become more elongated. Furthermore, the design of out triculture condition introduced a new mechanical cue due to the presence of the astrocytes in the stroma layer and this further increased the relevance of our 3D platform. Furthermore, we investigated the influence of astrocytes on proliferation of GSCs and observed a significant increase in proliferation in the triculture conditions. Our platform also permitted the study of GSC phenotype using immunofluorescence studies. By staining for specific stemness and astrocytic differentiation markers, we confirmed that the GSCs maintained their stem-like phenotype even in the presence of the astrocytes.

Together, our findings prove that astrocytes influenced the proliferation of GSCs and thus, this platform can be used for further studies to investigate happenings at the genetic level.

4.2 FUTURE WORK

4.2.1 Molecular level mechanistic studies:

In our study, we investigated the migration, proliferation and morphological and phenotypical differences within well-defined experimental conditions with multicellular culture incorporating astrocytes into the stromal layer as well as a perivascular layer within our microfluidic platform. To further understand the contributions of astrocytes and perivascular niche on tumor progression, specific genes surrounding GSC survival and progression need to be studied. We intended to conduct an RNA-sequencing assay to study the upregulation/downregulation of specific genes like beta III tubulin and IL-8.

To do this, we have utilized Nattokinase, an enzyme for digesting the fibrin vascular layer to break the vascular layer barrier and permit access to the tumor layer containing the GB3 cells. After further optimization of fibrinolysis, we could proceed to digest the Matrigel® matrix and extract the GB3 cells and subsequently sort them using flow cytometry for further studies.

REFERENCES

Abou-Antoun, T. J., Hale, J. S., Lathia, J. D., & Dombrowski, S. M. (2017). Brain Cancer Stem Cells in Adults and Children: Cell Biology and Therapeutic Implications. *Neurotherapeutics, 14*(2), 372-384. doi:10.1007/s13311-017-0524-0

Ahmed, A. U., Auffinger, B., & Lesniak, M. S. (2013). Understanding glioma stem cells: rationale, clinical relevance and therapeutic strategies. *Expert Rev Neurother, 13*(5), 545-555. doi:10.1586/ern.13.42

Ayuso, J. M., Monge, R., Martinez-Gonzalez, A., Virumbrales-Munoz, M., Llamazares, G. A., Berganzo, J., . . . Fernandez, L. J. (2017). Glioblastoma on a microfluidic chip: Generating pseudopalisades and enhancing aggressiveness through blood vessel obstruction events. *Neuro Oncol, 19*(4), 503-513. doi:10.1093/neuonc/now230

Bahadur, S., Sahu, A. K., Baghel, P., & Saha, S. (2019). Current promising treatment strategy for glioblastoma multiform: A review. *Oncol Rev, 13*(2), 417. doi:10.4081/oncol.2019.417

Baxter, P. A., Lin, Q., Mao, H., Kogiso, M., Zhao, X., Liu, Z., . . . Li, X. N. (2014). Silencing BMI1 eliminates tumor formation of pediatric glioma CD133+ cells not by affecting known targets but by down-regulating a novel set of core genes. *Acta Neuropathol Commun, 2*, 160. doi:10.1186/s40478-014-0160-4

Bertassoni, L. E., Cecconi, M., Manoharan, V., Nikkhah, M., Hjortnaes, J., Cristino, A. L., . . . Khademhosseini, A. (2014). Hydrogel bioprinted microchannel networks for vascularization of tissue engineering constructs. *Lab Chip, 14*(13), 2202-2211. doi:10.1039/c4lc00030g

Calabrese, C., Poppleton, H., Kocak, M., Hogg, T. L., Fuller, C., Hamner, B., . . . Gilbertson, R. J. (2007). A perivascular niche for brain tumor stem cells. *Cancer Cell, 11*(1), 69-82. doi:10.1016/j.ccr.2006.11.020

Cha, C., Soman, P., Zhu, W., Nikkhah, M., Camci-Unal, G., Chen, S., & Khademhosseini, A. (2014). Structural Reinforcement of Cell-Laden Hydrogels with Microfabricated Three Dimensional Scaffolds. *Biomater Sci, 2*(5), 703-709. doi:10.1039/C3BM60210A

Chonan, Y., Taki, S., Sampetrean, O., Saya, H., & Sudo, R. (2017). Endothelium-induced three-dimensional invasion of heterogeneous glioma initiating cells in a microfluidic coculture platform. *Integr Biol (Camb), 9*(9), 762-773. doi:10.1039/c7ib00091j

Clement, V., Sanchez, P., de Tribolet, N., Radovanovic, I., & Ruiz i Altaba, A. (2007). HEDGEHOG-GLI1 signaling regulates human glioma growth, cancer stem cell self-renewal, and tumorigenicity. *Curr Biol, 17*(2), 165-172. doi:10.1016/j.cub.2006.11.033

Dolatshahi-Pirouz, A., Nikkhah, M., Kolind, K., Dokmeci, M. R., & Khademhosseini, A. (2011). Micro- and nanoengineering approaches to control stem cell-biomaterial interactions. *J Funct Biomater, 2*(3), 88-106. doi:10.3390/jfb2030088

Faria, J., Romao, L., Martins, S., Alves, T., Mendes, F. A., de Faria, G. P., . . . Moura Neto, V. (2006). Interactive properties of human glioblastoma cells with brain neurons in culture and neuronal modulation of glial laminin organization. *Differentiation, 74*(9-10), 562-572. doi:10.1111/j.1432-0436.2006.00090.x

Fidoamore, A., Cristiano, L., Antonosante, A., d'Angelo, M., Di Giacomo, E., Astarita, C., . . . Cimini, A. (2016). Glioblastoma Stem Cells Microenvironment: The Paracrine Roles of the Niche in Drug and Radioresistance. *Stem Cells Int, 2016*, 6809105. doi:10.1155/2016/6809105

Friedmann-Morvinski, D., & Verma, I. M. (2014). Dedifferentiation and reprogramming: origins of cancer stem cells. *EMBO Rep, 15*(3), 244-253. doi:10.1002/embr.201338254

Gravina, G. L., Mancini, A., Colapietro, A., Delle Monache, S., Sferra, R., Vitale, F., . . . Festuccia, C. (2019). The Small Molecule Ephrin Receptor Inhibitor, GLPG1790, Reduces Renewal Capabilities of Cancer Stem Cells, Showing Anti-Tumour Efficacy on Preclinical Glioblastoma Models. *Cancers (Basel), 11*(3). doi:10.3390/cancers11030359

Guan, X., Hasan, M. N., Maniar, S., Jia, W., & Sun, D. (2018). Reactive Astrocytes in Glioblastoma Multiforme. *Mol Neurobiol, 55*(8), 6927-6938. doi:10.1007/s12035-018-0880-8

Hambardzumyan, D., & Bergers, G. (2015). Glioblastoma: Defining Tumor Niches. *Trends Cancer, 1*(4), 252-265. doi:10.1016/j.trecan.2015.10.009

Hambardzumyan, D., Gutmann, D. H., & Kettenmann, H. (2016). The role of microglia and macrophages in glioma maintenance and progression. *Nat Neurosci, 19*(1), 20-27. doi:10.1038/nn.4185

Hanif, F., Muzaffar, K., Perveen, K., Malhi, S. M., & Simjee Sh, U. (2017). Glioblastoma Multiforme: A Review of its Epidemiology and Pathogenesis through Clinical Presentation and Treatment. *Asian Pac J Cancer Prev, 18*(1), 3-9. doi:10.22034/APJCP.2017.18.1.3

Heinrich, M. A., Bansal, R., Lammers, T., Zhang, Y. S., Michel Schiffelers, R., & Prakash, J. (2019). 3D-Bioprinted Mini-Brain: A Glioblastoma Model to Study Cellular Interactions and Therapeutics. *Adv Mater, 31*(14), e1806590. doi:10.1002/adma.201806590

Henrik Heiland, D., Ravi, V. M., Behringer, S. P., Frenking, J. H., Wurm, J., Joseph, K., . . . Schnell, O. (2019). Tumor-associated reactive astrocytes aid the evolution of immunosuppressive environment in glioblastoma. *Nat Commun, 10*(1), 2541. doi:10.1038/s41467-019-10493-6

Hira, V. V., Ploegmakers, K. J., Grevers, F., Verbovsek, U., Silvestre-Roig, C., Aronica, E., . . . Van Noorden, C. J. (2015). CD133+ and Nestin+ Glioma Stem-Like Cells Reside Around CD31+ Arterioles in Niches that Express SDF-1alpha, CXCR4, Osteopontin and Cathepsin K. *J Histochem Cytochem, 63*(7), 481-493. doi:10.1369/0022155415581689

Infanger, D. W., Cho, Y., Lopez, B. S., Mohanan, S., Liu, S. C., Gursel, D., . . . Fischbach, C. (2013). Glioblastoma stem cells are regulated by interleukin-8 signaling in a tumoral perivascular niche. *Cancer Res, 73*(23), 7079-7089. doi:10.1158/0008-5472.CAN-13-1355

Joo, K. M., Kim, J., Jin, J., Kim, M., Seol, H. J., Muradov, J., . . . Nam, D. H. (2013). Patient-specific orthotopic glioblastoma xenograft models recapitulate the histopathology and biology of human glioblastomas in situ. *Cell Rep, 3*(1), 260-273. doi:10.1016/j.celrep.2012.12.013

Kharaziha, M., Nikkhah, M., Shin, S. R., Annabi, N., Masoumi, N., Gaharwar, A. K., . . . Khademhosseini, A. (2013). PGS:Gelatin nanofibrous scaffolds with tunable mechanical and structural properties for engineering cardiac tissues. *Biomaterials, 34*(27), 6355-6366. doi:10.1016/j.biomaterials.2013.04.045

Kharaziha, M., Shin, S. R., Nikkhah, M., Topkaya, S. N., Masoumi, N., Annabi, N., . . . Khademhosseini, A. (2014). Tough and flexible CNT-polymeric hybrid scaffolds for engineering cardiac constructs. *Biomaterials, 35*(26), 7346-7354.

doi:10.1016/j.biomaterials.2014.05.014

Lin, Q., Liu, Z., Ling, F., & Xu, G. (2016). Astrocytes protect glioma cells from chemotherapy and upregulate survival genes via gap junctional communication. *Mol Med Rep, 13*(2), 1329-1335. doi:10.3892/mmr.2015.4680

Logun, M., Zhao, W., Mao, L., & Karumbaiah, L. (2018). Microfluidics in Malignant Glioma Research and Precision Medicine. *Adv Biosyst, 2*(5). doi:10.1002/adbi.201700221

Ma, Y., Yu, W., Shrivastava, A., Alemi, F., Lankachandra, K., Srivastava, R. K., & Shankar, S. (2017). Sanguinarine inhibits pancreatic cancer stem cell characteristics by inducing oxidative stress and suppressing sonic hedgehog-Gli-Nanog pathway. *Carcinogenesis, 38*(10), 1047-1056. doi:10.1093/carcin/bgx070

Mathiisen, T. M., Lehre, K. P., Danbolt, N. C., & Ottersen, O. P. (2010). The perivascular astroglial sheath provides a complete covering of the brain microvessels: an electron microscopic 3D reconstruction. *Glia, 58*(9), 1094-1103. doi:10.1002/glia.20990

Matias, D., Balca-Silva, J., da Graca, G. C., Wanjiru, C. M., Macharia, L. W., Nascimento, C. P., . . . Moura-Neto, V. (2018). Microglia/Astrocytes-Glioblastoma Crosstalk: Crucial Molecular Mechanisms and Microenvironmental Factors. *Front Cell Neurosci, 12*, 235. doi:10.3389/fncel.2018.00235

Matsuda, K., Sato, A., Okada, M., Shibuya, K., Seino, S., Suzuki, K., . . . Kitanaka, C. (2012). Targeting JNK for therapeutic depletion of stem-like glioblastoma cells. *Sci Rep, 2*, 516. doi:10.1038/srep00516

Memic, A., Navaei, A., Mirani, B., Cordova, J. A. V., Aldhahri, M., Dolatshahi-Pirouz, A., . . . Nikkhah, M. (2017). Bioprinting technologies for disease modeling. *Biotechnol Lett, 39*(9), 1279-1290. doi:10.1007/s10529-017-2360-z

Nagaraju, S., Truong, D., Mouneimne, G., & Nikkhah, M. (2018). Microfluidic Tumor-Vascular Model to Study Breast Cancer Cell Invasion and Intravasation. *Adv Healthc Mater, 7*(9), e1701257. doi:10.1002/adhm.201701257

Navaei, A., Moore, N., Sullivan, R. T., Truong, D., Migrino, R. Q., & Nikkhah, M. (2017). Electrically conductive hydrogel-based micro-topographies for the development of organized cardiac tissues. *RSC Advances, 7*(6), 3302-3312. doi:10.1039/c6ra26279a

Navaei, A., Rahmani Eliato, K., Ros, R., Migrino, R. Q., Willis, B. C., & Nikkhah, M. (2019). The influence of electrically conductive and non-conductive nanocomposite scaffolds on the maturation and excitability of engineered cardiac tissues. *Biomater Sci, 7*(2), 585-595. doi:10.1039/c8bm01050a

Navaei, A., Saini, H., Christenson, W., Sullivan, R. T., Ros, R., & Nikkhah, M. (2016). Gold nanorod-incorporated gelatin-based conductive hydrogels for engineering cardiac tissue constructs. *Acta Biomater, 41*, 133-146. doi:10.1016/j.actbio.2016.05.027

Navaei, A., Truong, D., Heffernan, J., Cutts, J., Brafman, D., Sirianni, R. W., . . . Nikkhah, M. (2016). PNIPAAm-based biohybrid injectable hydrogel for cardiac tissue engineering. *Acta Biomater, 32*, 10-23. doi:10.1016/j.actbio.2015.12.019

Nikkhah, M., Eshak, N., Zorlutuna, P., Annabi, N., Castello, M., Kim, K., . . . Khademhosseini, A. (2012). Directed endothelial cell morphogenesis in micropatterned gelatin methacrylate hydrogels. *Biomaterials, 33*(35), 9009-9018. doi:10.1016/j.biomaterials.2012.08.068

Nikkhah, M., Strobl, J. S., & Agah, M. (2009). Attachment and response of human fibroblast and breast cancer cells to three dimensional silicon microstructures of different geometries. *Biomed Microdevices, 11*(2), 429-441. doi:10.1007/s10544-008-9249-5

Nikkhah, M., Strobl, J. S., De Vita, R., & Agah, M. (2010). The cytoskeletal organization of breast carcinoma and fibroblast cells inside three dimensional (3-D) isotropic silicon microstructures. *Biomaterials, 31*(16), 4552-4561. doi:10.1016/j.biomaterials.2010.02.034

Nikkhah, M., Strobl, J. S., Peddi, B., & Agah, M. (2009). Cytoskeletal role in differential adhesion patterns of normal fibroblasts and breast cancer cells inside silicon microenvironments. *Biomed Microdevices, 11*(3), 585-595. doi:10.1007/s10544-008-9268-2

Nikkhah, M., Strobl, J. S., Schmelz, E. M., & Agah, M. (2011). Evaluation of the influence of growth medium composition on cell elasticity. *J Biomech, 44*(4), 762-766. doi:10.1016/j.jbiomech.2010.11.002

Nikkhah, M., Strobl, J. S., Schmelz, E. M., Roberts, P. C., Zhou, H., & Agah, M. (2011). MCF10A and MDA-MB-231 human breast basal epithelial cell co-culture in silicon micro-arrays. *Biomaterials, 32*(30), 7625-7632. doi:10.1016/j.biomaterials.2011.06.041

Okada, M., Sangadala, S., Liu, Y., Yoshida, M., Reddy, B. V., Titus, L., & Boden, S. D. (2009). Development and optimization of a cell-based assay for the selection of synthetic compounds that potentiate bone morphogenetic protein-2 activity. *Cell Biochem Funct, 27*(8), 526-534. doi:10.1002/cbf.1615

Omuro, A., & DeAngelis, L. M. (2013). Glioblastoma and other malignant gliomas: a clinical review. *JAMA, 310*(17), 1842-1850. doi:10.1001/jama.2013.280319

Pal, A., Smith, C. I., Palade, J., Nagaraju, S., Alarcon-Benedetto, B. A., Kilbourne, J., . . . Nikkhah, M. (2020). Poly(N-isopropylacrylamide)-based dual-crosslinking biohybrid injectable hydrogels for vascularization. *Acta Biomater, 107*, 138-151. doi:10.1016/j.actbio.2020.02.041

Pal, A., Vernon, B. L., & Nikkhah, M. (2018). Therapeutic neovascularization promoted by injectable hydrogels. *Bioact Mater, 3*(4), 389-400. doi:10.1016/j.bioactmat.2018.05.002

Pedde, R. D., Mirani, B., Navaei, A., Styan, T., Wong, S., Mehrali, M., . . . Akbari, M. (2017). Emerging Biofabrication Strategies for Engineering Complex Tissue Constructs. *Adv Mater, 29*(19). doi:10.1002/adma.201606061

Peela, N., Barrientos, E. S., Truong, D., Mouneimne, G., & Nikkhah, M. (2017). Effect of suberoylanilide hydroxamic acid (SAHA) on breast cancer cells within a tumor-stroma microfluidic model. *Integr Biol (Camb), 9*(12), 988-999. doi:10.1039/c7ib00180k

Peela, N., Sam, F. S., Christenson, W., Truong, D., Watson, A. W., Mouneimne, G., . . . Nikkhah, M. (2016). A three dimensional micropatterned tumor model for breast cancer cell migration studies. *Biomaterials, 81*, 72-83. doi:10.1016/j.biomaterials.2015.11.039

Peela, N., Truong, D., Saini, H., Chu, H., Mashaghi, S., Ham, S. L., . . . Nikkhah, M. (2017). Advanced biomaterials and microengineering technologies to recapitulate the stepwise process of cancer metastasis. *Biomaterials, 133*, 176-207. doi:10.1016/j.biomaterials.2017.04.017

Phillips, H. S., Kharbanda, S., Chen, R., Forrest, W. F., Soriano, R. H., Wu, T. D., . . . Aldape, K. (2006). Molecular subclasses of high-grade glioma predict prognosis, delineate a pattern of disease progression, and resemble stages in neurogenesis. *Cancer Cell, 9*(3), 157-173. doi:10.1016/j.ccr.2006.02.019

Plaks, V., Kong, N., & Werb, Z. (2015). The cancer stem cell niche: how essential is the niche in regulating stemness of tumor cells? *Cell Stem Cell, 16*(3), 225-238. doi:10.1016/j.stem.2015.02.015

Polyak, K., & Hahn, W. C. (2006). Roots and stems: stem cells in cancer. *Nat Med, 12*(3), 296-300. doi:10.1038/nm1379

Rath, B. H., Fair, J. M., Jamal, M., Camphausen, K., & Tofilon, P. J. (2013). Astrocytes enhance the invasion potential of glioblastoma stem-like cells. *PLoS One, 8*(1), e54752. doi:10.1371/journal.pone.0054752

Saini, H., Navaei, A., Van Putten, A., & Nikkhah, M. (2015). 3D cardiac microtissues encapsulated with the co-culture of cardiomyocytes and cardiac fibroblasts. *Adv Healthc Mater, 4*(13), 1961-1971. doi:10.1002/adhm.201500331

Saini, H., Rahmani Eliato, K., Silva, C., Allam, M., Mouneimne, G., Ros, R., & Nikkhah, M. (2018). The Role of Desmoplasia and Stromal Fibroblasts on Anti-cancer Drug Resistance in a Microengineered Tumor Model. *Cell Mol Bioeng, 11*(5), 419-433. doi:10.1007/s12195-018-0544-9

Saini, H., Rahmani Eliato, K., Veldhuizen, J., Zare, A., Allam, M., Silva, C., . . . Nikkhah, M. (2020). The role of tumor-stroma interactions on desmoplasia and tumorigenicity within a microengineered 3D platform. *Biomaterials, 247*, 119975. doi:10.1016/j.biomaterials.2020.119975

Sato, A., Sunayama, J., Okada, M., Watanabe, E., Seino, S., Shibuya, K., . . . Kitanaka, C. (2012). Glioma-initiating cell elimination by metformin activation of FOXO3 via AMPK. *Stem Cells Transl Med, 1*(11), 811-824. doi:10.5966/sctm.2012-0058

Sharifzad, F., Ghavami, S., Verdi, J., Mardpour, S., Mollapour Sisakht, M., Azizi, Z., . . . Hamidieh, A. A. (2019). Glioblastoma cancer stem cell biology: Potential theranostic targets. *Drug Resist Updat, 42*, 35-45. doi:10.1016/j.drup.2018.03.003

Shergalis, A., Bankhead, A., 3rd, Luesakul, U., Muangsin, N., & Neamati, N. (2018). Current Challenges and Opportunities in Treating Glioblastoma. *Pharmacol Rev, 70*(3), 412-445. doi:10.1124/pr.117.014944

Silver, D. J., & Lathia, J. D. (2018). Revealing the glioma cancer stem cell interactome, one niche at a time. *J Pathol, 244*(3), 260-264. doi:10.1002/path.5024

Strobl, J. S., Nikkhah, M., & Agah, M. (2010). Actions of the anti-cancer drug suberoylanilide hydroxamic acid (SAHA) on human breast cancer cytoarchitecture in silicon microstructures. *Biomaterials, 31*(27), 7043-7050. doi:10.1016/j.biomaterials.2010.05.023

Su, C., Li, D., Li, N., Du, Y., Yang, C., Bai, Y., . . . Zhang, Y. (2018). Studying the mechanism of PLAGL2 overexpression and its carcinogenic characteristics based on 3'-untranslated region in colorectal cancer. *Int J Oncol, 52*(5), 1479-1490. doi:10.3892/ijo.2018.4305

Taylor, O. G., Brzozowski, J. S., & Skelding, K. A. (2019). Glioblastoma Multiforme: An Overview of Emerging Therapeutic Targets. *Front Oncol, 9*, 963. doi:10.3389/fonc.2019.00963

Tessarz, P., & Kouzarides, T. (2014). Histone core modifications regulating nucleosome structure and dynamics. *Nat Rev Mol Cell Biol, 15*(11), 703-708. doi:10.1038/nrm3890

Truong, D., Fiorelli, R., Barrientos, E. S., Melendez, E. L., Sanai, N., Mehta, S., & Nikkhah, M. (2019).

A three-dimensional (3D) organotypic microfluidic model for glioma stem cells - Vascular interactions. *Biomaterials, 198*, 63-77. doi:10.1016/j.biomaterials.2018.07.048

Truong, D., Puleo, J., Llave, A., Mouneimne, G., Kamm, R. D., & Nikkhah, M. (2016). Breast Cancer Cell Invasion into a Three Dimensional Tumor-Stroma Microenvironment. *Sci Rep, 6*, 34094. doi:10.1038/srep34094

Truong, D. D., Kratz, A., Park, J. G., Barrientos, E. S., Saini, H., Nguyen, T., . . . Nikkhah, M. (2019). A Human Organotypic Microfluidic Tumor Model Permits Investigation of the Interplay between Patient-Derived Fibroblasts and Breast Cancer Cells. *Cancer Res, 79*(12), 3139-3151. doi:10.1158/0008-5472.CAN-18-2293

Ulasov, I. V., Nandi, S., Dey, M., Sonabend, A. M., & Lesniak, M. S. (2011). Inhibition of Sonic hedgehog and Notch pathways enhances sensitivity of CD133(+) glioma stem cells to temozolomide therapy. *Mol Med, 17*(1-2), 103-112. doi:10.2119/molmed.2010.00062

Wang, C., Li, J., Sinha, S., Peterson, A., Grant, G. A., & Yang, F. (2019). Mimicking brain tumor-vasculature microanatomical architecture via co-culture of brain tumor and endothelial cells in 3D hydrogels. *Biomaterials, 202*, 35-44. doi:10.1016/j.biomaterials.2019.02.024

Wang, M., Zhao, J., Zhang, L., Wei, F., Lian, Y., Wu, Y., . . . Guo, C. (2017). Role of tumor microenvironment in tumorigenesis. *J Cancer, 8*(5), 761-773. doi:10.7150/jca.17648

Wang, X., Phan, D. T., Sobrino, A., George, S. C., Hughes, C. C., & Lee, A. P. (2016). Engineering anastomosis between living capillary networks and endothelial cell-lined microfluidic channels. *Lab Chip, 16*(2), 282-290. doi:10.1039/c5lc01050k

Whiteside, T. L. (2008). The tumor microenvironment and its role in promoting tumor growth. *Oncogene, 27*(45), 5904-5912. doi:10.1038/onc.2008.271

Zbinden, M., Duquet, A., Lorente-Trigos, A., Ngwabyt, S. N., Borges, I., & Ruiz i Altaba, A. (2010). NANOG regulates glioma stem cells and is essential in vivo acting in a cross-functional network with GLI1 and p53. *EMBO J, 29*(15), 2659-2674. doi:10.1038/emboj.2010.137

Zorlutuna, P., Annabi, N., Camci-Unal, G., Nikkhah, M., Cha, J. M., Nichol, J. W., . . . Khademhosseini, A. (2012). Microfabricated biomaterials for engineering 3D tissues. *Adv Mater, 24*(14), 1782-1804. doi:10.1002/adma.201104631

Zuccarini, M., Giuliani, P., Ziberi, S., Carluccio, M., Iorio, P. D., Caciagli, F., & Ciccarelli, R. (2018). The Role of Wnt Signal in Glioblastoma Development and Progression: A Possible New Pharmacological Target for the Therapy of This Tumor. *Genes (Basel), 9*(2). doi:10.3390/genes9020105

APPENDIX A: COPYRIGHTS AND PERMISSION

Figure 1.1

Order Summary

Licensee:	525 South Forest Avenue
Order Date:	Apr 9, 2020
Order Number:	4805080250611
Publication:	Nature Reviews Materials
Title:	Dissecting and rebuilding the glioblastoma microenvironment with engineered materials
Type of Use:	Thesis/Dissertation
Order Total:	220.80 USD

Figure 1.2 A-C

Order Summary

Licensee:	525 South Forest Avenue
Order Date:	Apr 9, 2020
Order Number:	4805071466877
Publication:	Integrative Biology
Title:	Endothelium-induced three-dimensional invasion of heterogeneous glioma initiating cells in a microfluidic coculture platform
Type of Use:	Thesis/Dissertation
Order Total:	0.00 USD

Figure 1.2 D, E

Order Summary

Licensee:	525 South Forest Avenue
Order Date:	Apr 9, 2020
Order Number:	4805070932011
Publication:	Biomedical Microdevices
Title:	Engineered 3D tumour model for study of glioblastoma aggressiveness and drug evaluation on a detachably assembled microfluidic device
Type of Use:	Thesis/Dissertation
Order Total:	0.00 USD

Figure 1.3

Order Summary

Licensee:	525 South Forest Avenue
Order Date:	Apr 9, 2020
Order Number:	4805080250611
Publication:	Nature Reviews Materials
Title:	Dissecting and rebuilding the glioblastoma microenvironment with engineered materials
Type of Use:	Thesis/Dissertation
Order Total:	220.80 USD

Figure 1.3

Licensee:	525 South Forest Avenue
Order Date:	Apr 13, 2020
Order Number:	4806900171395
Publication:	Nature Biomedical Engineering
Title:	A bioprinted human-glioblastoma-on-a-chip for the identification of patient-specific responses to chemoradiotherapy
Type of Use:	Thesis/Dissertation
Order Total:	220.80 USD

Figure 1.4

Licensee:	525 South Forest Avenue
Order Date:	Apr 13, 2020
Order Number:	4806900620857
Publication:	Neuro-Oncology
Title:	Glioblastoma on a microfluidic chip: Generating pseudopalisades and enhancing aggressiveness through blood vessel obstruction events
Type of Use:	Thesis/Dissertation
Order Total:	0.00 USD

Figure 2.1

Order Summary

Licensee:	525 South Forest Avenue
Order Date:	Apr 9, 2020
Order Number:	4805080985330
Publication:	Advanced Healthcare Materials
Title:	Microfluidic Tumor–Vascular Model to Study Breast Cancer Cell Invasion and Intravasation
Type of Use:	Dissertation/Thesis
Order Total:	0.00 USD

Figure 2.2

Order Summary

Licensee:	525 South Forest Avenue
Order Date:	Apr 9, 2020
Order Number:	4805070539223
Publication:	Biomaterials
Title:	A three-dimensional (3D) organotypic microfluidic model for glioma stem cells – Vascular interactions
Type of Use:	reuse in a thesis/dissertation
Order Total:	0.00 USD

Figure 2.4

Order Summary

Licensee:	525 South Forest Avenue
Order Date:	Apr 9, 2020
Order Number:	4805080985330
Publication:	Advanced Healthcare Materials
Title:	Microfluidic Tumor–Vascular Model to Study Breast Cancer Cell Invasion and Intravasation
Type of Use:	Dissertation/Thesis
Order Total:	0.00 USD